CIAMTIS

U.S. DOT Region 3 University Transportation Center

Use of SmartRock Sensors to Monitor Pavement Condition for Supporting Maintenance Decision Making

April 2022

Prepared by:
Shihui Shen, The Pennsylvania State University;
Linbing Wang, Virginia Tech;
Cheng Zhang, The Pennsylvania State University;
Dylan Ildefonzo, Virginia Tech

r3utc.psu.edu

PennState
College of Engineering

LARSON
TRANSPORTATION
INSTITUTE

Disclaimer

Acknowledgement

Technical Report Documentation Page

1. Report No. CIAM-UTC-REG12	2. Government Accession No.	3. Recipient's Catalog No.	
4. Title and Subtitle Use of SmartRock Sensors to Monitor Pavement Condition for Supporting Maintenance Decision Making		**5. Report Date** April 2022	
		6. Performing Organization Code	
7. Author(s) Shihui Shen, https://orcid.org/0000-0002-5718-722X Linbing Wang, https://orcid.org/0000-0003-2670-376X Cheng Zhang, Dylan Ildefonzo		**8. Performing Organization Report No.**	
9. Performing Organization Name and Address The Pennsylvania State University Virginia Polytechnic Institute and State University 201 Transportation Research Building University Park, PA 16802-4710		**10. Work Unit No. (TRAIS)**	
		11. Contract or Grant No. 69A3551847103	
12. Sponsoring Agency Name and Address U.S. Department of Transportation Research and Innovative Technology Administration 3rd Fl, East Bldg E33-461 1200 New Jersey Ave, SE Washington, DC 20590		**13. Type of Report and Period Covered** Final Report 03/1/2019 – 03/1/2022	
		14. Sponsoring Agency Code	

16. Abstract

The in-situ modulus of asphalt mixtures directly determines the stress-strain relationships of asphalt pavement under external loading and its structural conditions. The evaluation of dynamic modulus over time has also been related to the deterioration of pavement performance. Although crucial, accurate determination of in-situ dynamic modulus has always been difficult. The most direct method is to take field cores and perform laboratory dynamic modulus tests, which damages the pavement. Non-destructive testing, as with the Falling Weight Deflectometer, can also obtain the modulus properties of the pavement periodically, yet the modulus data are scarce and the data collection process is time- and labor-intensive. With recent advancements in data science and sensing technologies, it is technologically promising to develop an efficient and reliable method of estimating the in-situ modulus; the development of such a method became the motivation of this study. This project studied the methodology of using particle-size wireless sensors to conduct in-situ dynamic modulus tests and collect data under vehicular loading. It then applied an artificial neural network (ANN) model to predict the in-situ pavement modulus and quantify vehicular speed. A variety of engineering responses, including triaxial stress and Euler angle, loading frequency, and pavement temperatures, were collected by the wireless sensors in three pavement sections and used as input data to develop the ANN model. Laboratory dynamic modulus tests and MMLS3 tests using the same material as the paving projects were also performed on specimens with embedded wireless sensors. Those laboratory data, in combination with a small portion of randomly selected early-stage field sensing data, were used as the training dataset for the development of the ANN model. The remaining field data were used to test the ANN model, using the laboratory dynamic modulus master curve as a reference. The results show that the developed ANN model, when adequately trained with particle-level sensing data, is feasible and robust to predict the in-situ dynamic modulus of asphalt pavement. Future studies are recommended to include more data on the material and pavement structure variations over extended service lives so that the in-situ modulus can be used to assess pavement conditions and support maintenance decision-making.

17. Key Words wireless sensor, in-situ, dynamic modulus, artificial neural network (ANN)		**18. Distribution Statement** No restrictions. This document is available from the National Technical Information Service, Springfield, VA 22161	
19. Security Classif. (of this report) Unclassified	**20. Security Classif. (of this page)** Unclassified	**21. No. of Pages** 49	**22. Price**

Form DOT F 1700.7   **(8-72)**   **Reproduction of completed page authorized**

Table of Contents

List of Figures

List of Tables

Introduction

BACKGROUND

The in-situ mechanical properties of pavement material are crucial for pavement design, performance prediction, and structural condition assessment. Dynamic modulus is a fundamental material property in the stress and strain response calculations and is a required input for performance prediction in mechanistic-empirical models (AASHTO, 2020). Research findings suggest that the pavement modulus deterioration has a consistent trend with fatigue cracking based on an analysis of Long-Term Pavement Performance (LTPP) database (Wang, et al. 2019). Furthermore, pavement performance, such as cracking, can be used to calculate the pavement condition index (PCI), which can provide an objective determination of pavement maintenance and rehabilitation (Boyapati and Kumar, 2015; Rahman and Tarefder, 2015).

However, efficient and accurate determination of in-situ dynamic modulus has always been a challenge. The in-place modulus can be obtained by the laboratory tests using field cores or the field nondestructive tests. The laboratory testing is complicated, costly, and time-consuming (Dao et al., 2020). Besides, the specimens are cored from the pavement, which can reduce the integrity and long-term performance of the pavement. The nondestructive tests are developed to obtain in-place modulus in the field. The falling weight deflectometer (FWD) test is one of the most widely used nondestructive tests. The deflection basins are used to backcalculate layer moduli and estimate the in-place structural condition of the pavement layers (AASHTO, 2020). The FWD test is a useful method to evaluate the in-place modulus, but it also has some inherent disadvantages. For example, the backcalculation result is not unique, and the deflection basin can be obtained by different modulus combinations (AASHTO, 2020). What is more, the impact loading of the FWD is different from the vehicular loading in terms of loading amplitude and frequencies, causing the estimated modulus to be higher than the modulus under vehicular loading (Cheng et al., 2021). Factors such as cost and time required for testing can also limit the use of the FWD tests, resulting in limited data for the pavement over the service life. Therefore, more and more studies are now concentrating on the application of advanced sensors to determine the in-situ mechanical properties. Jointly, artificial intelligence (AI) methods have also been introduced into the transportation infrastructure field to achieve higher accuracy of the model prediction. The next section will review applications of advanced sensors, particularly embedded sensors, and data analysis algorithms in pavement condition assessment.

LITERATURE REVIEW

Embedded sensors have been applied in pavement health monitoring for decades. There are a few types of the traditional sensors frequently used in embedded sensor monitoring systems. One of the most used sensor types are strain gauges, such as H-gauge, strip gage, optic fiber (OF) strain gauge, and Fiber Bragg grating (FBG) strain gauge (Tabatabaee and Sebaaly, 1990; Teral, 1992; Wang et al., 2014). H-gauge obtains strain by measuring the distance between the two anchors, and the output voltage changes with the variation of the distance (Sebaaly et al., 1995). Therefore, the accuracy of H-gauge is highly

CIAMTIS
U.S. DOT Region 3 University Transportation Center

dependent on the bonding, and the voltage signal is easily disturbed by the electromagnetic interference in the field. The OF and FBG strain gauges have the advantages of anti-electromagnetic interference and long-distance transmission (Teral, 1992). However, the installation of the OF and FBG sensor requires specialized multi-disciplinary technologies, including civil engineering, electrical engineering, and telecommunication engineering (Teral, 1992). Therefore, such strain gauges are mainly used in research projects. Besides strain gauges, piezoelectric sensors are widely employed in the weigh-in-motion system for monitoring deflection and vertical stress (Huff et al., 2005). Piezoelectric sensors are low cost and have low sensitivity to temperature, but high-quality installation is required to obtain acceptable monitoring accuracy (Iaquinta et al., 2004; Papagiannakis et al., 1989). Earth pressure cells (EPC) are designed to provide vertical stress measurements in soil (Theroux et al., 2001). The literature suggests that the stress values reported by EPC were higher than the actual values because of the arching phenomenon caused by the shape and material of the EPC (Islam et al., 2014). Above all, traditional sensors have some disadvantages for field monitoring, such as low monitoring accuracy, complicated installation processes, and less consideration of consistency between pavement material and sensors.

On the other hand, the concept of the Micro-Electromechanical Sensor (MEMS) was presented as early as the 1970s, and the sensors were utilized in various areas like the medical industry, automotive industry, and civil engineering (Sebaaly et al., 1995). Compared to traditional embedded sensors, MEMS represent a great improvement. Analog signals can be transformed to digital signals within the MEMS sensor so that the safety and stability of the communication are enhanced (Ceylan et al., 2013). Almost all MEMS are integrated with a wireless module. Wireless communication has significant advantages, including improved survivability, simplified installation and collection processes, and real-time monitoring during construction (Ceylan et al., 2013; Saafi and Romine, 2005; Liu et al., 2015). Owing to the tiny size of the sensor chip, the MEMS can be designed to satisfy the requirements of the pavement structure. Based on these advancements, the MEMS have been used in structural health monitoring (SHM), including on bridges, railroads (Liu et al., 2015), and pavements (Wang et al., 2019). MEMS technology can provide a large quantity of data from the SHM, making MEMS a promising trend for pavement health monitoring.

Another important issue in pavement health monitoring is the interpretation and analysis of collected data and the obtainment of reliable results to assist project management and decision-making. In traditional models, the modulus can be backcalculated by matching the collected data with the predicted deflection in the time domain or frequency domain (Uzan, 1994). The backcalculation procedure consists of the forward simulation and the backward procedure (Kutay et al., 2011). Based on the mechanistic theories, various mechanical models were developed to calculate the mechanical responses in forward simulation. The development of a mechanical model typically includes two steps: setting up the equations of the multi-layer pavement system and solving the equations according to the vehicle-pavement interaction condition and initial conditions. Under this subject, the elastic layer system has been developed and gradually improved since 1945 (Burmister, 1945). The asphalt mixture is treated as the viscoelastic-viscoplastic material in a multi-layer structure, and the mechanical responses of the pavement are dependent on the behaviors of the asphalt material, temperature, loading frequency, and other factors (Darabi et al., 2012). With the development of computational technologies, the finite element (FE) method has been widely used in the forward simulation. Machine learning algorithms, such as artificial neural networks (ANN), can be applied in backward processing. Combinations of FE and ANN to perform the forward and backward analysis in the time domain have shown promising results (Hamim et al., 2020).

In recent years, machine learning (ML) algorithms have been widely applied in pavement distress classification, performance prediction, and dynamic modulus backcalculation. Traditional distress classification methods are highly dependent on experience and can lead to subjective decision-making. Accordingly, various machine learning algorithms, such as multilayer perceptron (MLP), random forest

(RF) classifier, convolutional neural network (CNN), and support vector machine (SVM), were introduced to classify the pavement distresses based on the collected signals and images (Hoang et al., 2018; Praticò et al., 2020). Praticò et al. (2020) suggested based on their study that the SVM shows higher accuracy than other algorithms for the classification using the acceleration collected during field experiments. Furthermore, different hybrid models were developed to improve the prediction accuracy. The SVM and the artificial bee colony (ABC) optimization algorithms were integrated to increase classification accuracy (Hoang et al., 2018). Majidifard et al. (2020) combined the YOLO (you only look once) model and U-net model to classify the pavement distresses and quantify the severity of distresses excluding the dependency of objective judgment.

Machine learning algorithms were also utilized to predict the Pavement Condition Index (PCI) and International Roughness Index (IRI). Karballaeezadeh et al. (2020) introduced genetic algorithm (GA) optimization into the RF model to predict the PCI and IRI based on the LTPP database. Damirchilo et al. (2021) studied the extreme gradient boosting (XGBoost) that was developed based on the decision tree method to predict the PCI and IRI. The XGBoost model had an advantage of handling the LTPP dataset with missing data (Damirchilo et al., 2021). Zeiada et al. (2020) trained and tested different machine learning models using the LTPP database. The results showed that the ANN model was the most accurate model among the regression tree, the SVM, ensembles, and Gaussian process regression (GPR) (Zeiada et al., 2020).

The ANN model can be used to backcalculate the dynamic modulus based on the FWD test. Two types of ANN model, multilayer feed-forward neural (MLFN) network and radial basis function network (RBFN), were compared using the FWD deflection history data. The results show that RBFN is more accurate than MLFN (Hamim et al., 2020). Wang et al. (2019) developed an Artificial Neural Network–Genetic Algorithm (ANN-GA) program to backcalculate the dynamic modulus with the FWD test. The ANN-GA showed higher accuracy than the traditional regression approach (Wang et al., 2019). Above all, machine learning algorithms have been demonstrated to be effective in predicting pavement performance and mechanical properties under various scenarios. Such methods could be promising for estimating the in-situ dynamic modulus based on the data collected by the embedded sensors. This project further explores these methodologies.

OBJECTIVES

This project aimed to develop an in-situ dynamic modulus predictive model by integrating sensing technology and machine learning algorithms. Such a model will be implemented for pavement condition evaluation and aid pavement maintenance decision making. Specifically, this project (1) develops data collection and analysis strategies for particle-sized wireless sensors for roadway applications; (2) develops methodologies to determine traffic information using embedded sensors; and (3) develops a data-informed approach to estimate the in-situ dynamic modulus and its deterioration trend under vehicular traffic loading.

Methodology

In this project, an in-situ dynamic modulus predictive model is developed with an artificial neural network algorithm based on the sensing data; the overall project methodology is illustrated in Figure 1. Aggregate-sized wireless sensors, called SmartRock, are applied to collect mechanical responses in the laboratory and the field. With the aid of SmartRock as a data sensing and collecting system, in-situ mechanical tests are realized under field climate and traffic conditions. At the same time, SmartRock sensor is embedded in the laboratory specimens to collect data during the dynamic modulus tests and the Model Mobile Load Simulator 1/3 Scale (MMLS3) test.

Both the field and lab data are used to train, validate, and test the ANN model. The validated predictive model can predict the in-situ dynamic modulus using the input data collected by the SmartRock sensors at different pavement service stages. The curve of dynamic modulus deterioration can hence provide data-informed support for maintenance decision-making.
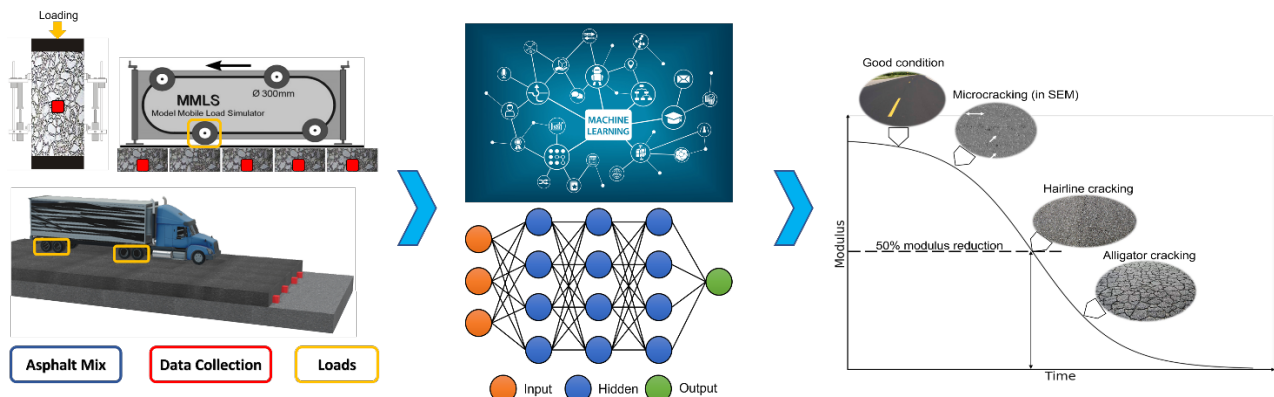
Figure 1. Framework of the methodology

C H A P T E R 3

Experiments

INTRODUCTION

Laboratory and field experiments were conducted to build a database that can be used to train, validate, and test the machine learning model. A novel wireless sensor, SmartRock, was utilized to record the mechanical responses in the material. In the laboratory, the dynamic modulus test was conducted to build a database of the dynamic modulus, while the SmartRock sensors that were embedded in the specimens recorded the mechanical responses during the test procedure. The MMLS3 accelerated tests were conducted to calibrate the predictive model over extended loading periods. In the field, SmartRock sensors were installed in the pavement to collect in-place pavement response data under traffic loads so that the in-situ modulus could be predicted using the predictive model.

SMARTROCK SENSOR

SmartRock (Figure 2) is a novel wireless particle sensor. In this project, the selected SmartRock is a cubic shape, multi-function sensor with the side length of 27 mm, which is close to the size of a coarse aggregate. High-temperature-resistant thermoplastic polymer materials are 3D printed as the external shell to protect SmartRock from moisture and high-temperature environments (120-150 ºC). SmartRock can record real-time triaxial acceleration, triaxial rotation, and three-dimensional pressure, temperature, and time. The data are transmitted to the adapter system via Bluetooth Low Energy (BLE) technology. SmartRock has a "sleep mode" (low energy consuming mode) function that can dramatically extend the battery life. SmartRock can be controlled by the adapter system to set sampling frequency, range, and automatic collection modes. Table 1 shows some basic parameters of the SmartRock. More technical details of the SmartRock can be referred to (Wang et al., 2019; Zhang et al., 2021).

SmartRock has prominent advantages in convenience, durability, reusability, and stability in contrast to traditional sensors. SmartRock sensors have been utilized to quantify ballast particle movement, including the peak vertical and horizontal accelerations, and angular acceleration during ballast deformation in railroads (Liu et al., 2015). They have also been used to monitor the compaction process of asphalt pavement by tracing the particle movement characteristics, including both rotation and acceleration (Wang et al., 2018). Therefore, the SmartRock monitoring system was selected in this study to collect data.
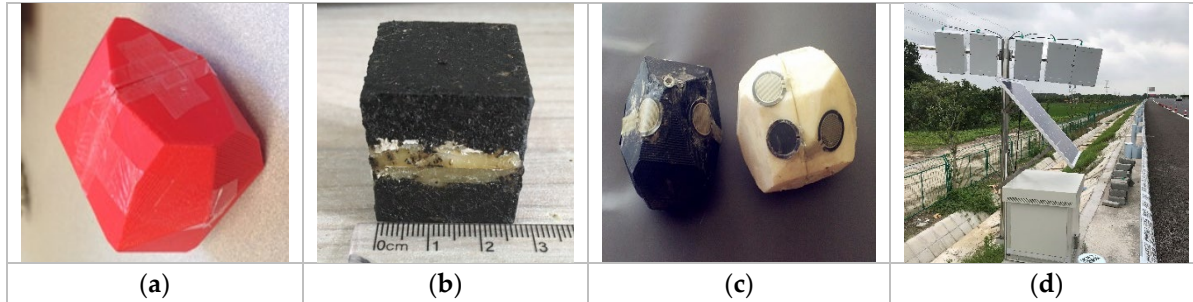
Figure 2. SmartRock sensors: (a) 3D printed SmartRock; (b) size of cubic shape SmartRock; (c) aggregate-like SmartRock; (d) wireless data acquisition (DAQ).

Table 1. SmartRock parameters

Properties	Parameters
Size	27*27*27 mm
Weight	43 g
Stress range	Triaxial, 1-100 lb
Orientation range	Triaxial, 360 °C
Accelerometer	Triaxial, ±2/±4/±8/±16 g
Gyroscope	Triaxial, ±250/±500/ ±1000/±2000 °/sec
Magnetometer	Triaxial, ±4800 uT
Sampling rate	0~200 Hz
Temperature range	0~150 °C

MATERIALS

Five mixtures from different projects were tested in the laboratory to build a database for training, validating, and testing the predictive model. The basic mix design information and gradation information of the five mixtures are presented in Table 2 and Figure 3. The No. 1, 2, 3, and 5 mixtures were plant-mixed, laboratory-compacted (PMLC) mixtures. The No. 4 mixture had same design as No. 3 but was blended in the laboratory (lab-mixed, lab-compacted LMLC mixtures) and aged for 2 hours to simulate short-term aging in accordance with AASHTO T 240. The No. 3 and No. 4 mixtures were used in the MMLS3 test. The No. 3 and No. 5 mixtures were also used in the field paving projects, in which SmartRock sensors were installed to collect data under vehicular loadings.

Table 2. Mix designs of the asphalt mixtures

No.	Asphalt Mix Type	Binder Grade	Binder Content (Pb)	Anti-strip Agent	RAP	Gyrations at N Design	Air Voids at N Design	Mixing and Compaction
1	SMA 12.5	PG 76-22	6.90%	0.50%	0	100	4.00%	PMLC
2	HMA 12.5	PG 64-22	5.80%	0.30%	15%	75	4.00%	PMLC
3	WMA 9.5	PG 64E-22	5.90%	0.25%	15%	100	4.00%	PMLC
4	WMA 9.5	PG 64E-22	5.90%	0.25%	15%	100	4.00%	LMLC
5	WMA 9.5	PG 64E-22	6.10%	0.25%	15%	75	4.00%	PMLC
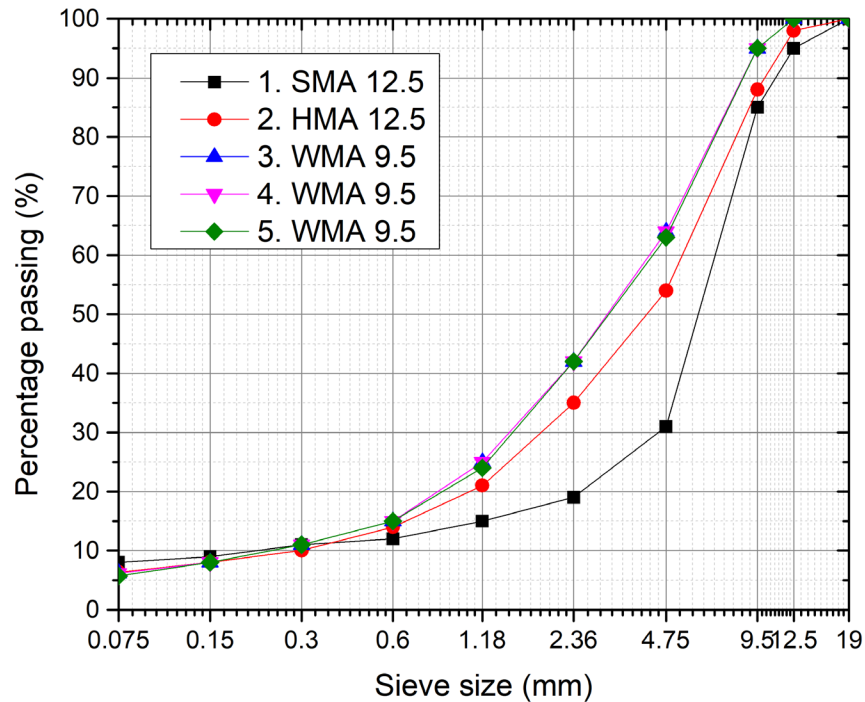
Figure 3. Gradation of the 5 mixtures

DYNAMIC MODULUS TEST

Dynamic modulus tests were conducted to obtain the master curve of the dynamic modulus for each mixture. All mixtures were compacted with the Superpave gyratory compactor. The specimens (Table 3) were compacted into 150 mm in height and 150 mm in diameter, and then cored into 100 mm in diameter as the final specimens. The target air void of the specimen was 7.0 ± 0.5 percent. In some specimens, one SmartRock sensor was embedded in the middle of the specimen to collect the mechanical response during the dynamic modulus test. These specimens were not tested for bulk specific gravity to avoid potential moisture damage to the SmartRock sensor electronics.

The dynamic modulus test of the mixtures was conducted in the MTS testing machine in accordance with AASHTO T342-11 (2019). The shape of the loading was sinusoid, the loading frequencies were selected as 0.1 Hz, 0.5 Hz, 1 Hz, 5 Hz, 10 Hz, and 25 Hz, and the temperatures were at 5 ºC, 10 ºC, 25 ºC, and 35 ºC degrees. Each mixture had two parallel specimens, whose average relative standard deviation of dynamic modulus is about 5%. Figure 4 shows the specimen with embedded SmartRock in the dynamic modulus test. The software can show the movement of the SmartRock in the specimen in real-time.

Table 3. Specimens of dynamic modulus test

Specimen	Asphalt Mix	Mixing and Compaction	SmartRock	Air Voids (%)
1-1	1 - SMA 12.5	PMLC	1	N/A*
1-2	1 - SMA 12.5	PMLC	1	N/A*
1-3	1 - SMA 12.5	PMLC	0	6.95
1-4	1 - SMA 12.5	PMLC	0	6.74
2-1	2 - HMA 12.5	PMLC	1	N/A*
2-2	2 - HMA 12.5	PMLC	1	N/A*
3-1	3 - WMA 9.5	PMLC	1	N/A*
3-2	3 - WMA 9.5	PMLC	1	N/A*
4-1	4 - WMA 9.5	LMLC	0	7.20
5-1	5 - WMA 9.5	PMLC	1	N/A*
5-2	5 - WMA 9.5	PMLC	0	6.91
5-3	5 - WMA 9.5	PMLC	1	N/A*

*N/A: This specimen was not tested for bulk specific gravity to avoid potential moisture damage to the electronics.
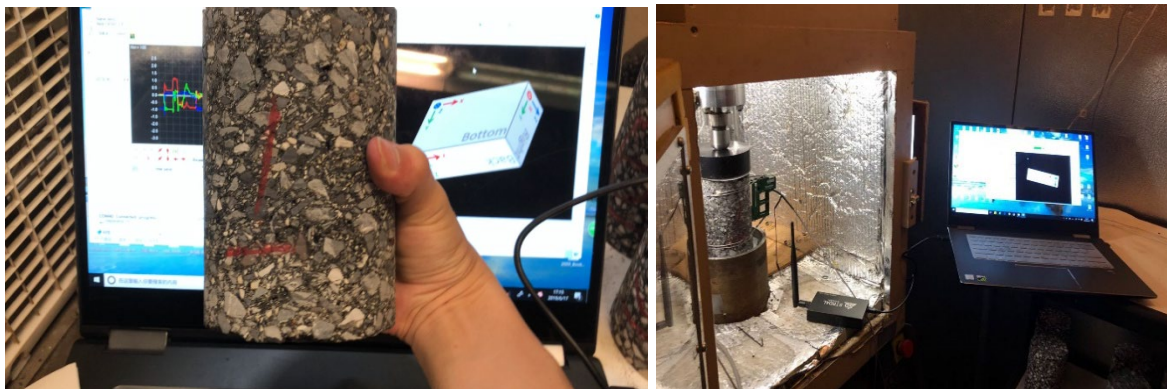
Figure 4. Dynamic modulus test with SmartRock sensor

MMLS3 TEST

The MMLS3 tests is an effective method to calibrate the predictive model. In the MMLS3 test, parameters, such as loading speed, tire pressure, loading weight, and number of loading passes are controlled. The collected data are used to verify the calculation of loading amplitude and loading frequency, and to calibrate the predictive model.

In this test, five specimens were installed in the loading frame. All specimens were placed on top of a thin rubber membrane to prevent lateral or longitudinal translation under the machine's loading. Four specimens, numbered L1, F3, F4, and L5, were embedded with SmartRock sensors to collect data. Two specimens, F3 and L5, contained surface-mounted MEMS accelerometers, as shown in Figure 5. In the figure, specimens embedded with SmartRock sensors are within the red boxes, and specimens with surface-mounted accelerometers are marked with blue circles.
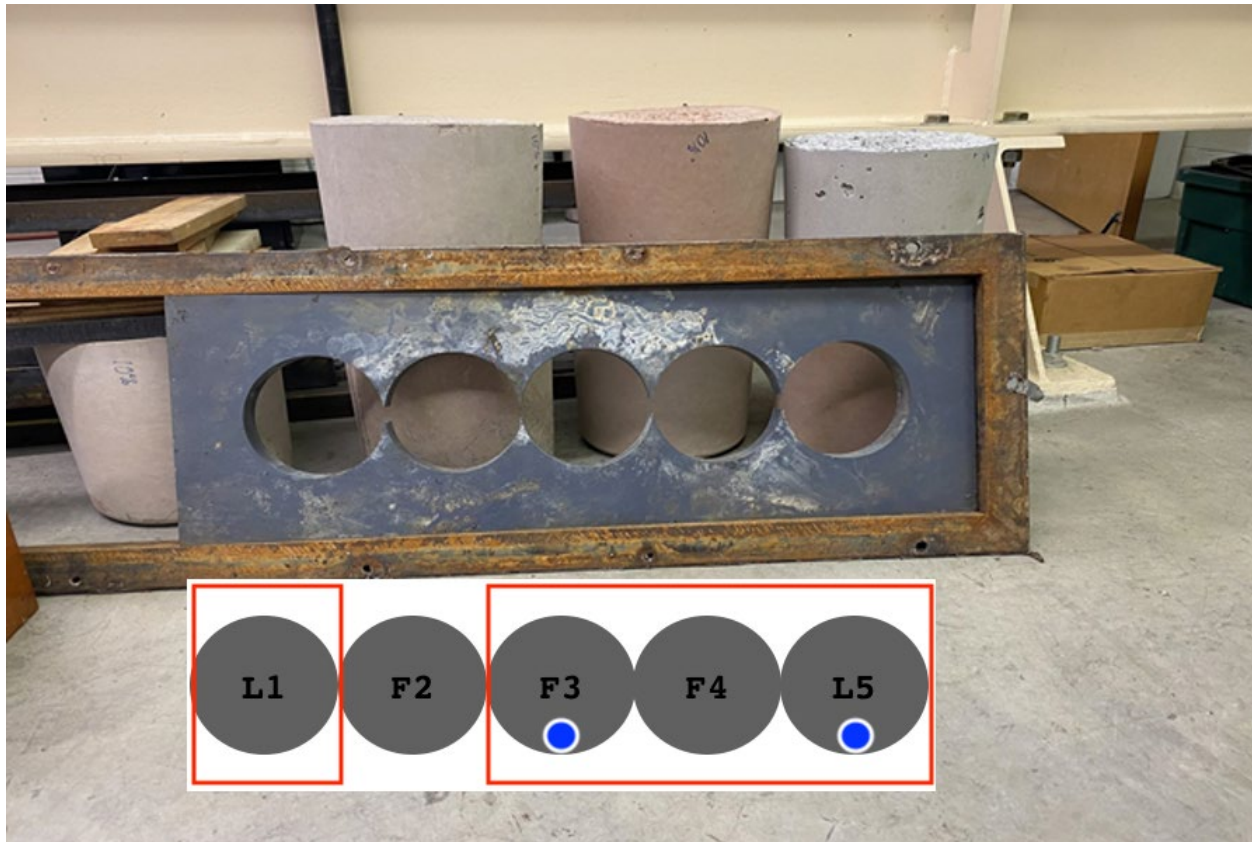
Figure 5. Specimen holding frame and specimen layout

The MMLS3 (Figure 6) was set up step by step. First, the machine was raised and the steel isolation plate was slid underneath and then bolted to the existing threaded openings in the floor. The bolts were tightened to prevent movement of the steel isolation plate under loading. Next, the specimen holder frame was installed on top of the isolation plate and secured in place using an additional set of bolts. Then, the plastic specimen holder with 5 holes was inserted into the holding frame. The thin rubber membranes were placed in the openings, and then the specimens were placed on top of the membranes. After that, the machine was lowered into place and the tire pressure was set using an air compressor; the pressure was measured using a digital pressure gauge. Once the desired tire pressure was reached, the machine load cell was put in place, and the bogie load (wheel load) at each wheel was measured and adjusted to the desired value by adjusting the suspension springs.

Figure 6. MMLS3 at Virginia Tech

The testing procedure included two parts: the short-term (parametric) loading test and the long-term loading test. In the short-term test, independent variables of the loading were adjusted parametrically to simulate the mechanical response of the specimens under different traffic conditions. Then, the long-term test was performed to collect data corresponding to pavement modulus deterioration under load repetitions for an extended period of time. For this test, the MMLS3 was to be run until severe distress of one or more specimens was noted, or until the allotted time period for the experiment expired. Both the short-term and the long-term test were performed at 22 °C.

The MMLS3 is capable of simulating a variety of different loading conditions through the adjustment of several independent variables that are related to physical parameters of the machine components. Independent variables that can be adjusted include:

- Speed in Axles/Hour (Range: 10 Hz = 150 axle/hr to 48 Hz = 7,200 axle/hr)

- Tire Pressure (200-500 kPa)

- Bogie Loading (1,700-2,100 Newton)

For the short-term (parametric) loading test, these variables were systematically adjusted to create eight different loading configurations. The configurations developed for the short-term test are shown in Tables 4-6.

Table 4. Independent variable: Loading speed

Run Number	Speed	Number of Loading Passes
1	20 Hz ± 2 Hz	100
2	30 Hz ± 2 Hz	100
3	40 Hz ± 2 Hz	100

For the independent variable of loading speed, the wander is set to ±0 mm from center, bogie load is set to 2.10 ± 0.05 kN, and tire pressure is set to 415 ± 20 kPa.

Table 5. Independent variable: Tire pressure

Run Number	Tire Pressure Level	Number of Loading Passes
4	415 ± 20 kPa	100
5	345 kPa ± 20 kPa	100
6	275 kPa ± 20 kPa	100

For the independent variable of tire pressure, the wander is set to ±0 mm from center, the loading speed is set to 25 ± 2 Hz, and bogie load is set to 2.10 ± 0.05 kN.

Table 6. Independent variable: Bogie load

Run Number	Bogie Load	Number of Loading Passes
7	2.10 kN ± 0.05 kN	100
8	2.30 kN ± 0.05 kN	100

For the independent variable of bogie load, the wander is set to ±0 mm from center, the tire pressure is set at 415 ± 20 kPa, and the loading speed is set at 25 ± 2 Hz.

As seen in Tables 4 through 6, each loading condition corresponded to a single "run" of the machine. Each run corresponded to 100 loading passes (wheel loads) onto the specimens, for a total of 800 loading passes over the course of the short-term test. For each run, acceleration, temperature, and time data were collected using both the specimen-embedded SmartRock sensors and the surface-mounted MEMS accelerometers. Additionally, the SmartRock sensors collected orientation and stress data.

For the long-term test, it was determined that the loading parameters needed to remain consistent across the entire span of testing. Accordingly, the loading conditions for the short-term test were reviewed and a neutral loading condition, that is a condition in which each loading parameter was set to the approximate middle of its potential value range, was selected. The long-term testing loading condition thus consisted of the following selected parameters:

- Loading Speed: 24 Hz motor speed = 1 bogie/second = 3,600 bogies/hr = 1.5 m/s

- Bogie Load: 2.10 kN (±0.05 kN)

- Tire Pressure: 700 kPa (±7.0 kPa)

The long-term testing schedule is shown in Table 7. At the end of each testing period, the ultrasonic pulse velocity (UPV) method, a non-destructive test (NDT) method, was conducted on each specimen to measure the ultrasonic pulse propagation time. The specimens were also measured using high-precision calipers before the completion of the UPV tests. The specimen size and ultrasonic pulse propagation time were used to calculate the ultrasonic pulse velocity, which was then correlated to obtain the dynamic modulus deterioration over the span of the experiment. In the UPV method, the pulse generator created

65,000 Hz electrical impulse. The electrical impulse is sent to the transmitter, which converts the pulse into an elastic impulse, which then propagates as elastic waves through the specimen. The receiver on the other side of the specimen receives the mechanical energy of the propagating elastic waves, and the time for the waves to pass through the specimen is measured electronically. The dynamic modulus can be calculated from the ultrasonic pulse velocity using Equations (1) and (2) (Dimter, et al. 2016):

$$E^* = \rho V^2 \frac{(1+\gamma)(1-2\gamma)}{1-\gamma} \tag{1}$$

$$V = \frac{L}{T} \tag{2}$$

Where: E^* is the dynamic modulus, ρ is the density, V is the ultrasounic pulse velocity, γ is the Poisson ratio, L is the specimen length over which the UPV test was conducted, and T is the travel time of ultrasound through the specimen.

For this experiment, the UPV method was conducted across the specimen, with the transmitter placed on the upper face and the receiver on the lower face. This topology was chosen due to ease of access of the tested surfaces, and also to remain consistent with the nature in which the specimen was loaded. Accordingly, in this case, the value of L in Equation (2) represents the measured thickness of the specimen.

Table 7. Long-term testing schedule

Date	Number of Wheel Loads
03 September 2021	3,518
07 September 2021	6,253
09 September 2021	9,112
10 September 2021	7,581
14 September 2021	2,657
16 September 2021	2,510
22 September 2021	1,404
27 September 2021	6,492
28 September 2021	5,121
30 September 2021	8,905
05 October 2021	8,981
12 October 2021	3,464
13 October 2021	5,718
Total:	71,716

FIELD TEST

Eight SmartRock sensors were installed in two overlay paving projects located in Altoona, Pennsylvania to collect the mechanical responses of the asphalt mixture. Each project used four SmartRocks. These projects are referred as Project A and Project B, respectively, in this report.

Project A

The field test was a pavement maintenance project located in Altoona, Pennsylvania. The original pavement surface was milled out by 2.5 inches, followed by two layers of overlay (a 1-inch leveling course plus a 1.5-inch wearing course). The wearing course mixture is a PG 64E-22 warm mix asphalt (WMA) mixture with nominal maximum aggregate size of 9.5 mm (mixture no. 3 in Table 1). The design

traffic level is 0.3 to 3 million equivalent single axle loads (ESALs). Figure 7 shows the SmartRock configuration in the pavement. Four SmartRock sensors (#2, #3, #5, #6) were embedded at the bottom of the wearing course during the construction, with two (#3 and #5) at the wheel path and two (#2 and #6) at 30 cm away from the wheel path. After opening traffic, SmartRock collected 30 min of stress data at 16:00 every Wednesday from 12 August 2020 to 23 September 2020. The temperature in the pavement ranged from 31 °C to 48 °C during the testing period. At the same time, a speed radar was used to measure the vehicle speed as a reference for the traffic speed analysis.
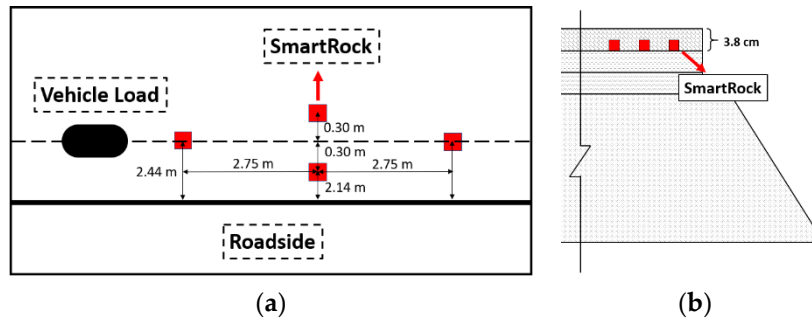
Figure 7. The configuration of the field test: (a) top view; (b) side view.

Project B

Project B is also a pavement maintenance project located in Altoona, Pennsylvania. The SmartRocks were installed at the bottom of the 1.5-inch surface layer. Four SmartRocks were located on the vertices of a rectangle with the long and short side of 2 ft and 1 ft, respectively, as shown in Figure 8. During the field experiments, SmartRocks were woken up to collect data for one-half hour every week from July 20, 2021, to August 31, 2021 (i.e., 7 weeks). After that, the schedule was changed to collect data for one-half hour every two weeks from August 31, 2021, to October 12, 2021 (i.e., 6 weeks) to extend the monitoring period.
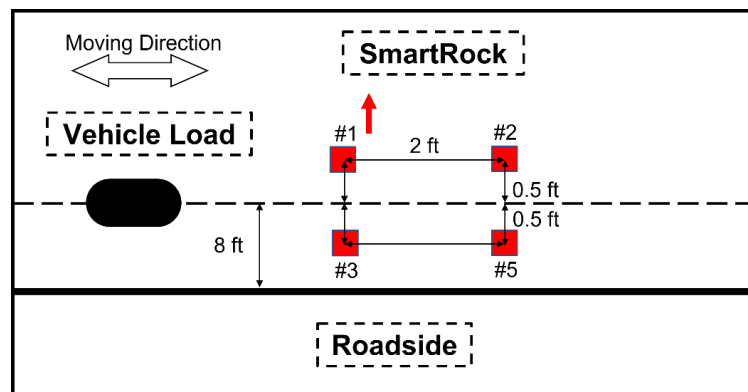
Figure 8. SmartRock installation configuration for field project B

CHAPTER 4

Pre-analysis

SmartRock sensors were used to collect the mechanical response in the laboratory and field test. It is worth noting that noise is inevitable in the collected data, especially in the field. Therefore, it was necessary to peform some pre-analysis on the collected data to remove noise and extract useful information as the inputs of the predictive model. The effect of SmartRock sensor on the results of dynamic modulus test should also be evaluated.

EFFECT OF SMARTROCK ON DYNAMIC MODULUS

The dynamic modulus master curves of four specimens produced by the same mixture 1-SMA 12.5 are shown in Figure 9. In particular, the SmartRocks were embedded in the middle of specimens 1-1, 1-2, while no SmartRocks were installed in specimens 1-3 and 1-4. As shown in Figure 9, the master curves of the specimens with SmartRocks are slightly lower than the ones without SmartRocks, but all four master curves follow a similar trend. It is thus reasonable to assume that the SmartRock sensor has little effect on the dynamic modulus of the asphalt mixture.

U.S. DOT Region 3 University Transportation Center
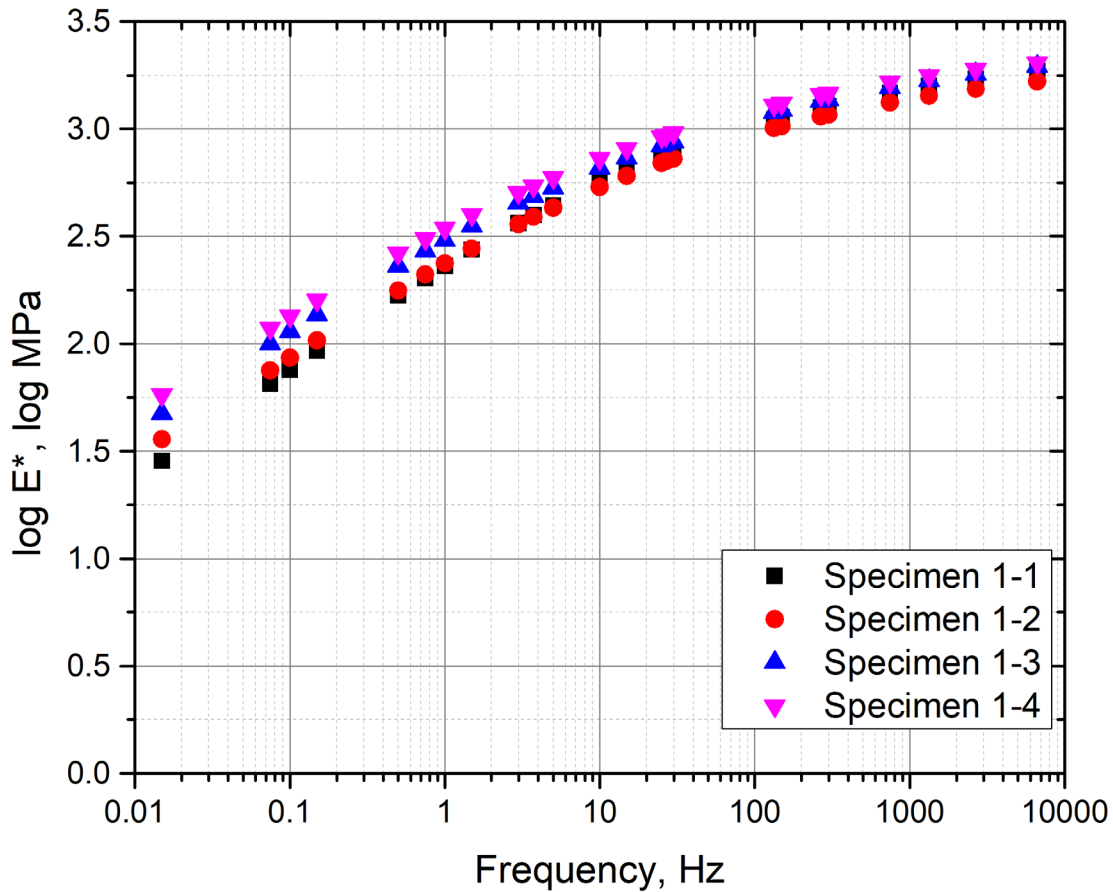
Figure 9. Master curve of the mixture 1 - SMA 12.5

LABORATORY DATA PRE-ANALYSIS

A variety of data have been collected by SmartRock sensors in laboratory and field tests, including triaxial stress, triaxial Euler angle, and triaxial acceleration. In the dynamic modulus test, the collected data showed sine wave signals. For example, Figure 10 shows the vertical stress collected by SmartRock at 25 °C, 10 Hz in the dynamic modulus test. At the beginning of the test, the trend line of stress slightly increases, and then the stress shows a sine wave signal. Accordingly, the frequency of the vertical stress can be calculated by the fast Fourier transform (FFT). Figure 11 shows the vertical stress in the MMLS3 test. Loading frequency was 20 Hz ± 2 Hz and bogie load was set to 2.10 ± 0.05 kN. The vertical stress was a periodical impulse signal that can be simplified to a half sine impulse signal when calculating the frequency with the FFT. The amplitudes and the frequencies were calculated as inputs of the predictive model.
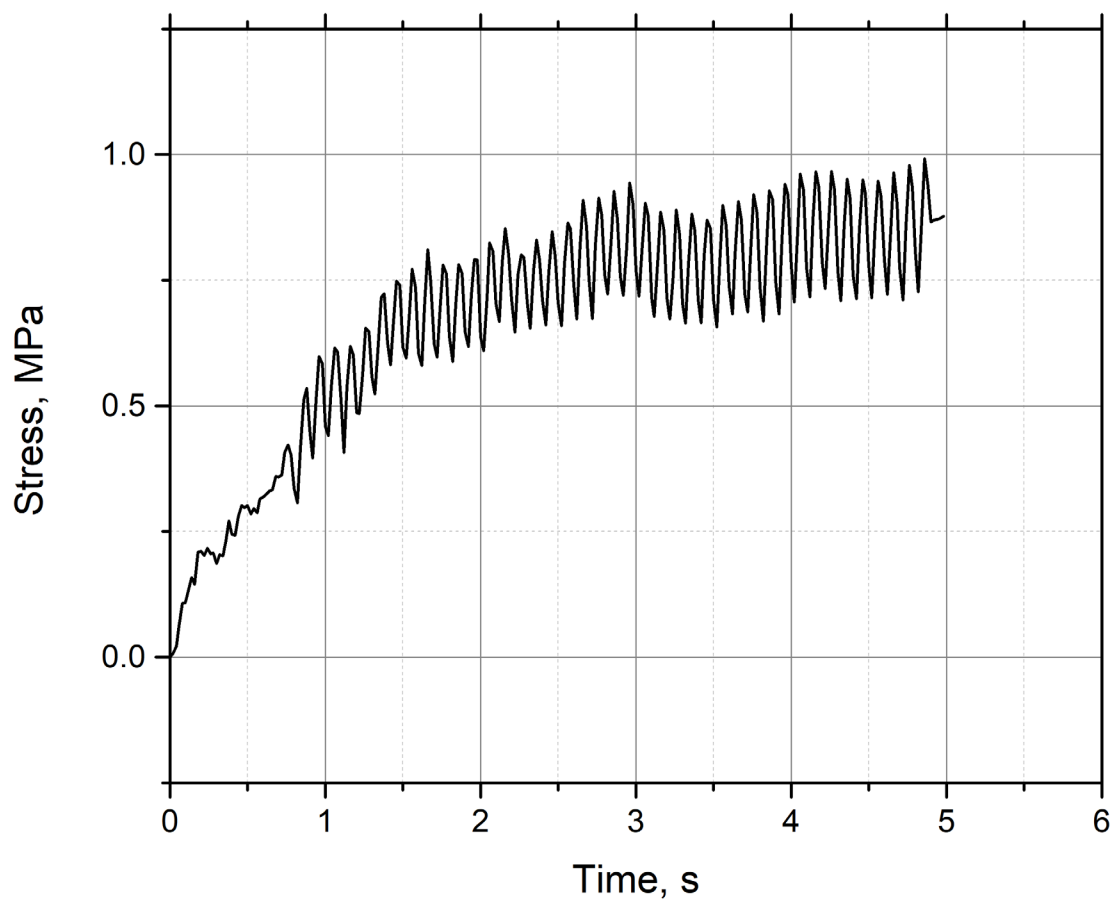
Figure 10. Vertical stress of SmartRock data in dynamic modulus test
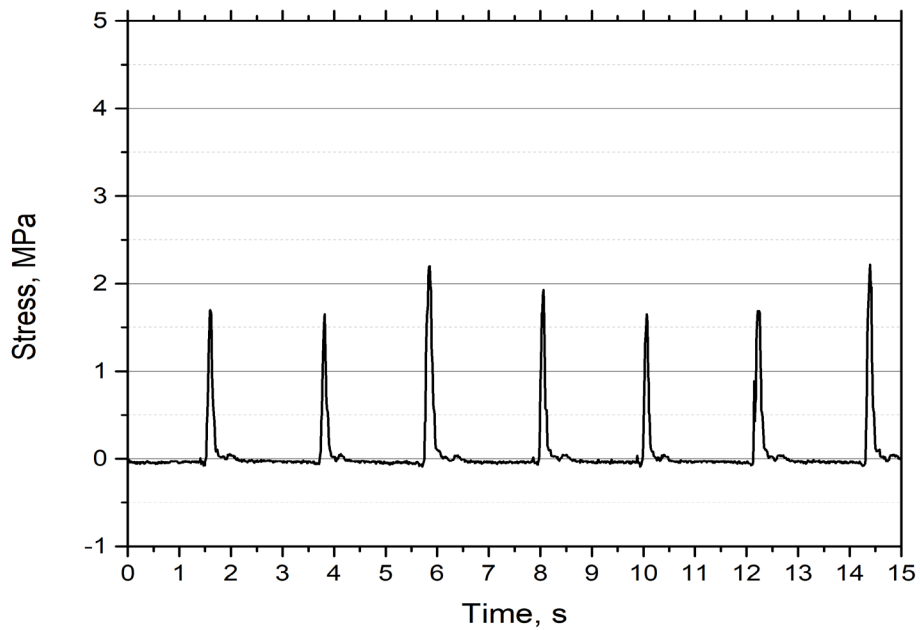
Figure 11. Vertical stress of SmartRock data in MMLS3 test

FIELD DATA PRE-ANALYSIS

In the field test, each vehicular loading can excite a range of vibration modes at different frequencies that are dependent on the load power. Obtaining the frequencies and the amplitudes of the signals in field experiments is more complicated than laboratory testing. Figure 12 shows an example of the in-situ vertical stress data collected by SmartRock from the project B in Altoona at 16:06, August 03, 2021.
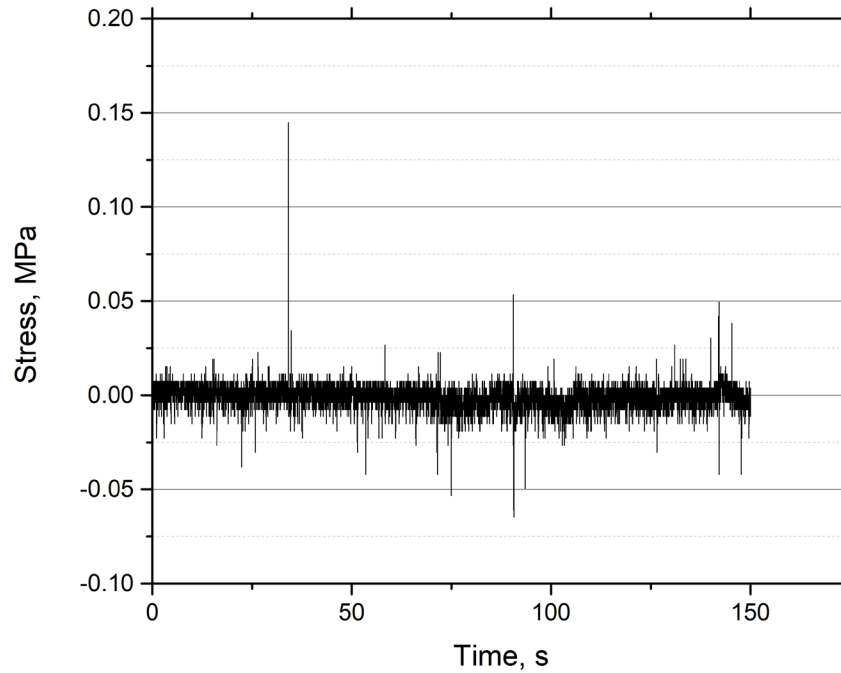
Figure 12. Vertical stress of SmartRock data in the field test

From Figure 12, some vertical stress responses are contaminated by noise. Several steps were used in this study to filter and clean the noise. Before filtering the noise and calculating the responses, the stationary of the signal should be analyzed. For the wide-sense stationary process, its mean and autocorrelation functions must be time invariant, namely:

$$E\big(X(t)\big) \equiv C \tag{3}$$

$$R_\sigma(t_1 + T, t_2 + T) = R_\sigma(t_1, t_2), \qquad \forall\, T \in R \tag{4}$$

Where: $E\big(X(t)\big)$ is the mean of a random process $X(t)$; C is a constant; $R_\sigma(t_1, t_2)$ is the correlation function; t_1, t_2 are time; and T is the time interval. From Equation (3), the moving average $m(t)$ should also be constant, namely:

$$E\big(X(t)\big) = m(t) \equiv C \tag{5}$$

Set the stress signal as $\sigma(t)$, its mean:

$$E = E\big(\sigma(t)\big) = -0.290 \ \text{MPa}$$

Calculate the moving average:

$$m(t_1) = -0.291 \ \text{MPa},$$
$$m(t_2) = -0.289 \ \text{MPa}.$$

$$E\big(\sigma(t)\big) \neq m\ (t_1) \neq m\ (t_2) \tag{6}$$

Where: t_1 is the first 150 s interval; t_2 is the second 150 s interval. From Equation (6), the mean of the signal is not a constant. Because the FFT is unable to express the time-frequency local properties (Zhou et al., 2009), the signal is considered as non-stationary. The empirical mode decomposition (EMD) method is thus used to filter the noises and to decompose the signal to different intrinsic mode functions, as shown in Figure 13 (van Jaarsveldt et al., 2021). The instantaneous frequency of intrinsic mode can be calculated by Hilbert Huang transformation (HHT). The amplitudes and frequencies of the intrinsic mode can be extracted as inputs of the ANN model to predict the in-situ dynamic modulus.
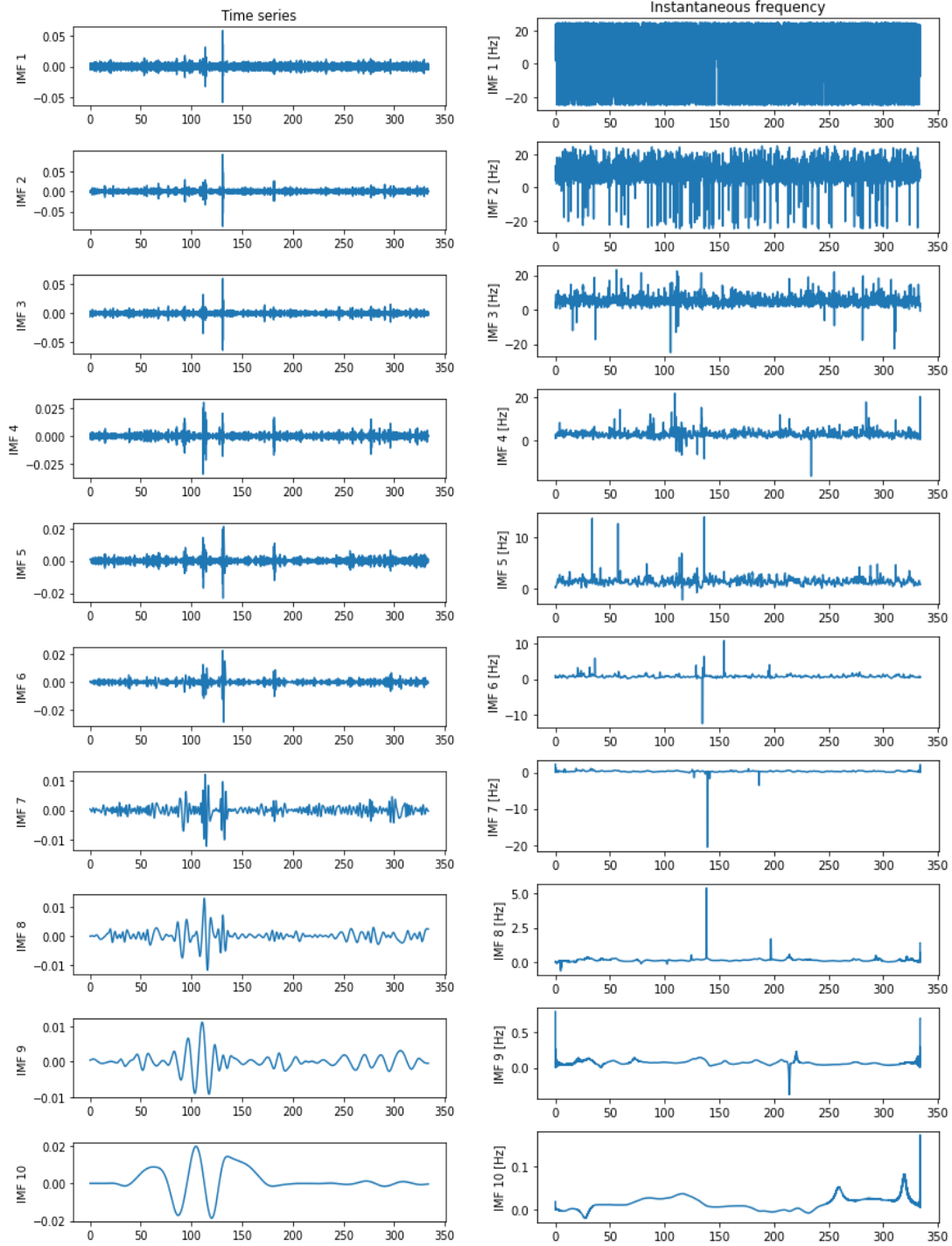
Figure 13. Intrinsic mode and the HHT

U.S. DOT Region 3 University Transportation Center

CHAPTER 5

Traffic Information Identification

INTRODUCTION

Traffic information, including but not limited to traffic volume, vehicle speed, and axle load, is one of the most important input factors for pavement design, management, and health monitoring. It also has a crucial influence on the performance of asphalt pavement. SmartRock sensors can be used to collect in-situ mechanical responses under vehicular loadings. The collected data can not only be applied to obtain the in-situ mechanical properties but can also be used to calculate the traffic speed. The loading speed is correlated to the duration of impulse and the dominant frequency that has a crucial impact on the dynamic modulus (Al-Qadi et al., 2008).

METHODOLOGY

In the field, the speed can be calculated with the distance between two sensors divided by the time delay between the two signals. The time delay is a critical parameter to determine the speed, since the distance can be measured directly. In this study, the cross-correlation method is used to determine the time-delay and three cross-correlation algorithms are applied and compared to increase the estimation accuracy of the time-delay. The cross-correlation method has been used in motion estimation, health assessment (Mo et al., 2018), and the passive SONAR array system (Ismaili Alaoui and Ibn-Elhaj, 2017). Various algorithms have been developed to estimate the time delay for different signals based on the cross-correlation method. Knapp and Carter (1976) discussed the commonly used algorithm such as Roth impulse response, smoothed coherence transform (SCOT), phase transform (PHAT), Eckart, and so on. In this paper, three algorithms of the cross-correlation method are described and used to calculate loading speed. The cross-correlation that is the overlapped area of two signals can indicate the similarity of the different signals, as shown in Equation 2:

$$R_{xy} = \int_{-\infty}^{+\infty} f(t)g(t + \tau)dt, \tag{7}$$

Where, R_{xy} is the cross-correlation, $f(t)$ and $g(t+\tau)$ are signals, and τ is the lag.

From Equation (7), the cross-correlation can be calculated at different lags τ. The maximum value of the cross-correlation can be found at a certain lag τ that is the time delay between the two signals.

In the signal generation and propagation, it is unavoidable that the signal is mixed with noises that have a significant influence on the cross-correlation results. So various algorithms were developed to reduce the effects of noises. The collected data can be assumed to consist of the signal and the noise, as shown in Equations (8) and (9):

$$f(t) = s_1(t) + n_1(t), \tag{8}$$

$$g(t) = s_2(t) + n_2(t), \tag{9}$$

Where: $s_1(t)$ and $s_2(t)$ are the signals; $n_1(t)$ and $n_2(t)$ are the noises. If $n_1(t)$ and $n_2(t)$ are independent, the $n_1(t)$ and $n_2(t)$ are the independent noises. Otherwise, they are correlated noises.

The SCOT algorithm and the PHAT algorithm are applied in this study to remove the correlated and independent noises and obtain an accurate cross-correlation calculation.

The stability and accuracy of the cross-correlation algorithms are evaluated based on the signal-noise-ratio (SNR) and the relative error (RE). The SNR can be defined as Equation (10) (Spagnolini, 2018):

$$SNR = \frac{A^2}{2\sigma^2}, \tag{10}$$

Where A and σ are the amplitude and standard deviation of the data. The SNR will increase with the noise components decreasing. For the cross-correlation algorithm, the higher SNR is, the more noises are filtered, and the better stability the algorithm has. The RE can be calculated by Equation (11):

$$RE = \frac{|U-V|}{V}, \tag{11}$$

Where U is the estimated velocity, and V is the measured velocity. A smaller number of RE indicates a higher accuracy of the estimation.

The Normalized Cross-Correlation (NCC) Algorithm

In practice, the NCC algorithm (Equation (12)) is a widely used cross-correlation algorithm without considering noises. The main advantage of the NCC is that it is less sensitive to linear changes in the amplitude of signals (Tsai and Lin, 2003):

$$NCC(\tau) = \frac{R_{xy}(\tau)}{\sqrt{\sigma_x \sigma_y}}, \tag{12}$$

Where: σ_x and σ_y are the standard deviation of the signal $f(t)$ and signal $g(t)$.

The SCOT Algorithm

The SCOT algorithm was developed to determine time delays between weak broad-band correlated noises received at two sensors (Carter et al., 1973):

$$R_{xy}(\tau) = \int_{-\infty}^{+\infty} G_{xy}(f)w(f)e^{2i\pi f\tau}df, \tag{13}$$

Where:

$$w(f) = \frac{G_{xy}(f)}{\sqrt{G_x(f)G_y(f)}}, \tag{14}$$

$G_x(f)$ and $G_y(f)$ are the auto spectra of signals $x(t)$ and $y(t)$. $G_{xy}(f)$ is the cross spectra. The correlated noises can be filtered by this algorithm. Furthermore, if the SNR of the SCOT results are larger than the SNR of the NCC results, the correlated noise should be considered as a part of noises. However, when the noises are independent, the weight function (Equation (14)) exhibits spreading. So, the SCOT algorithm can be used to calculate the cross-correlation of the signals with the correlated noises.

The PHAT Algorithm

For the independent noises, the PHAT algorithm can be used to avoid spreading. The calculation process is the same as the SCOT algorithm, while the weight function is defined as shown in Equation (15):

$$w(f) = \frac{1}{|G_{xy}(f)|}, \tag{15}$$

As with the SCOT algorithm, if the SNR of the PHAT results is larger than that of the NCC results, the independent noise should be considered. In addition, the type of noise can be decided by comparing the SNR of the SCOT algorithm and the PHAT algorithm.

In summary, the SCOT algorithm and the PHAT algorithm can remove the correlated and independent noises, respectively. The type of noise in the pavement can also be recognized by comparing the results of both algorithms.

RESULTS AND ANALYSIS

The vertical stress signals collected by two SmartRocks were utilized to calculate the loading speed. In the MMLS3 test, the distance between the two SmartRocks is 12 inches. Figure 14 shows a section of the stress signals (under the 2.10 ± 0.05 kN, 20 ± 2 Hz loads) extracted from the two SmartRocks. The sampling frequency is 200 Hz. When the load is approaching and leaving, the vertical stress rapidly increases to the peak value followed by a stress recovery. The data collected from different SmartRocks can be separated and matched directly, since the loading velocity and the wheel path were fixed.
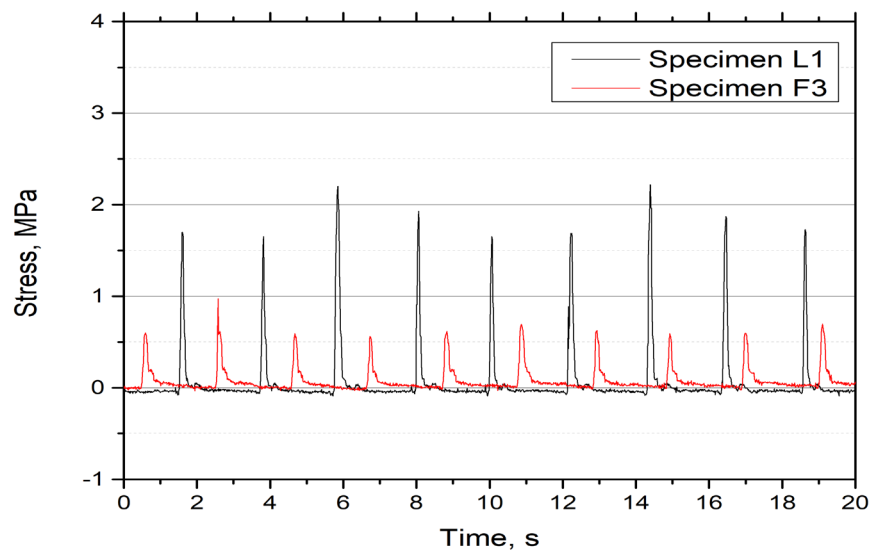

**Figure 14.** An example of the collected vertical stress in the MMLS3 experiment

In field project A, the distance between the two SmartRocks is 5.5 m. A series of signals under the vehicle loads were extracted from SmartRocks #3 and #5 (Figure 15a). It was found that although there are different scenarios when the signals are very different (Figure 15b-15e), the trend of individual signal is similar to the signals collected from the MMLS3 test. Most cases belong to case 1, of which both two-axle loads of a vehicle were captured by two SmartRocks, and the time delay can be accurately calculated using the cross-correlation method, as shown in Figure 14b. In case 2 (Figure 15c), one of the SmartRocks (for example, SmartRock #5) only captured an axle load of the vehicle, while the SmartRock #3 captured two axle loads. Case 3 (Figure 15d) shows that two SmartRocks captured one axle load, respectively. These phenomena made it difficult to determine the specific axle load that caused the corresponding peak stress and could result in theoretical errors in case 2 and case 3. Figure 15e shows that only one SmartRock captured a vehicle load. In this case, the data were removed in the calculation because the time delay is hard to obtain from an individual SmartRock.
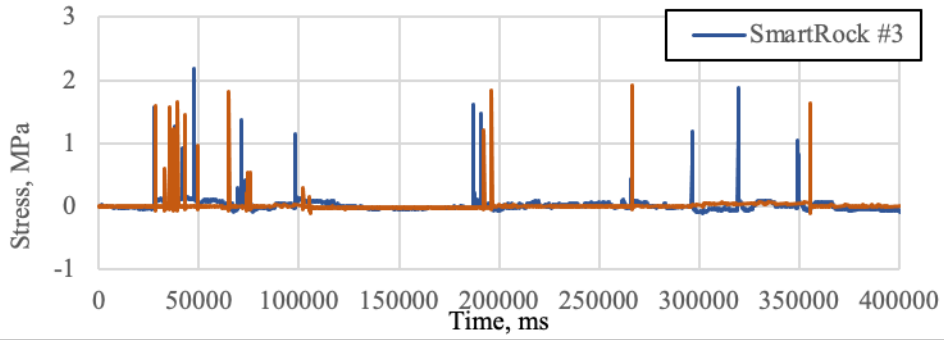
(a)
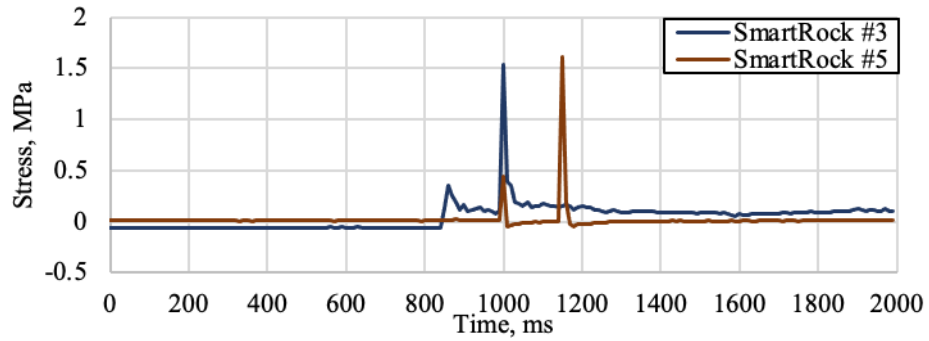
(b)
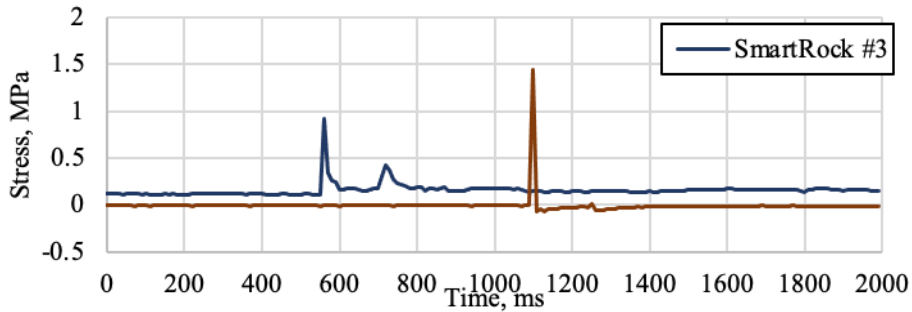
(c)
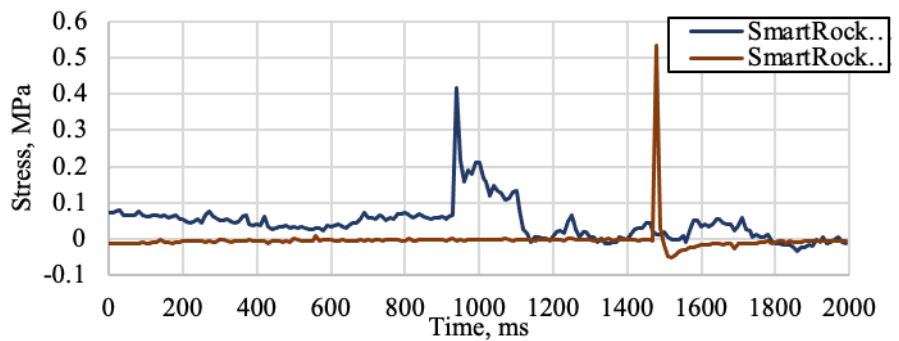
(d)
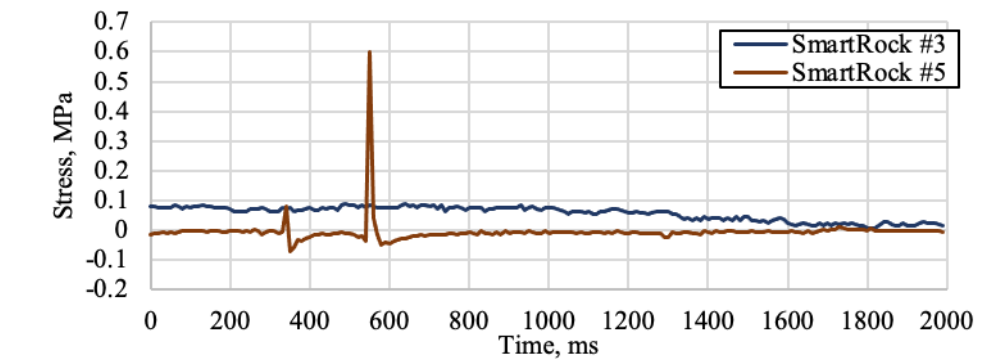
(e)

Figure 15. Collected stress signals in the field: (a) a series of stress signals; (b) case 1, two SmartRocks captured two axle loads, respectively; (c) case 2, one of the SmartRocks only captured an axle load; (d) case 3, two SmartRocks captured an axle load, respectively; and (e) case 4, one of the SmartRock didn't capture the signals.

In the field, there are few peaks of cross-correlation for each vehicle (Figure 16). The time delay is supposed to be the lag location of the maximum cross-correlation value. The speed can hence be estimated using the determined time delay and the distance between two SmartRock sensors (5.5 m in the field test).
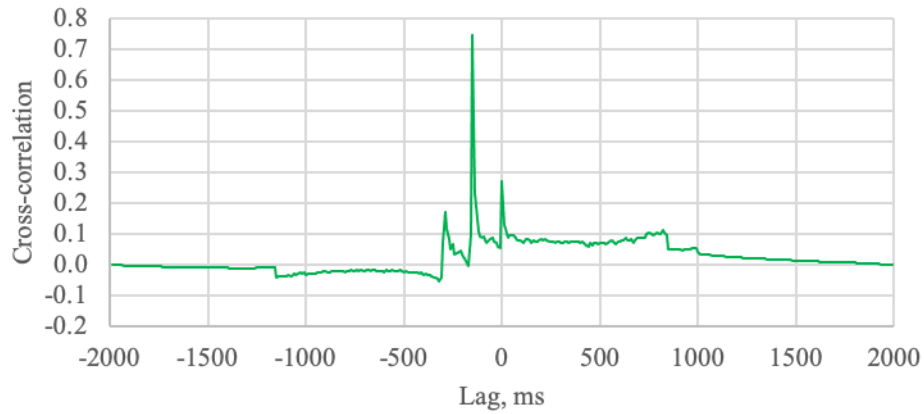
(a)
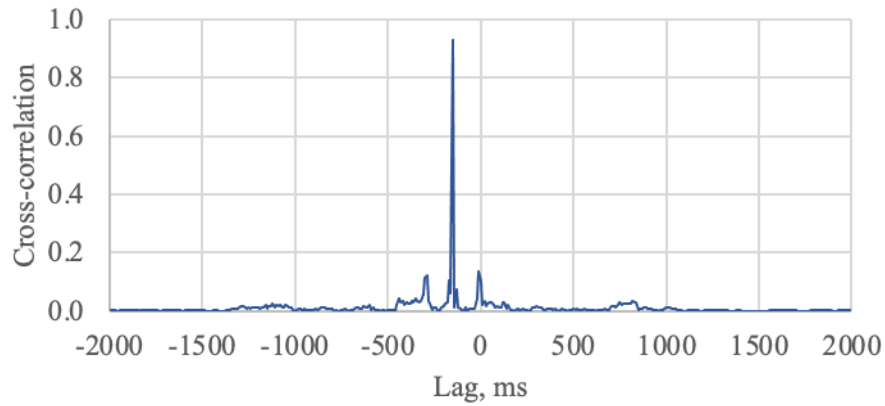
(b)
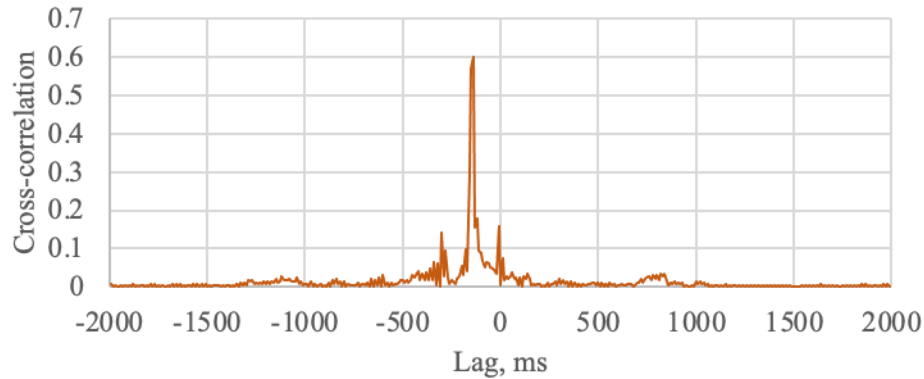
(c)

Figure 16. An example of the cross-correlation results for field test: (a) the NCC algorithm, (b) the PHAT algorithm, (c) the SCOT algorithm

Figure 17 presents a comparison between the estimated speed using different cross-correlation algorithms and the measured speeds, based on the project A data. A set of 20% error lines were also included in the figure to show the prediction quality. In general, most data points are within the 20% error lines and the

CIAMTIS

U.S. DOT Region 3 University Transportation Center

three algorithms seem to give reasonable estimation for the speeds. Large errors do happen in some cases, which may be related to the data-capturing capability of the existing sensor setup for sophisticated traffic conditions. In addition, the SCOT algorithm has the least points beyond the 20% error zone, indicating it might be the most promising algorithm among the three. A quantitative error analysis of these three algorithms will be discussed in the next section.
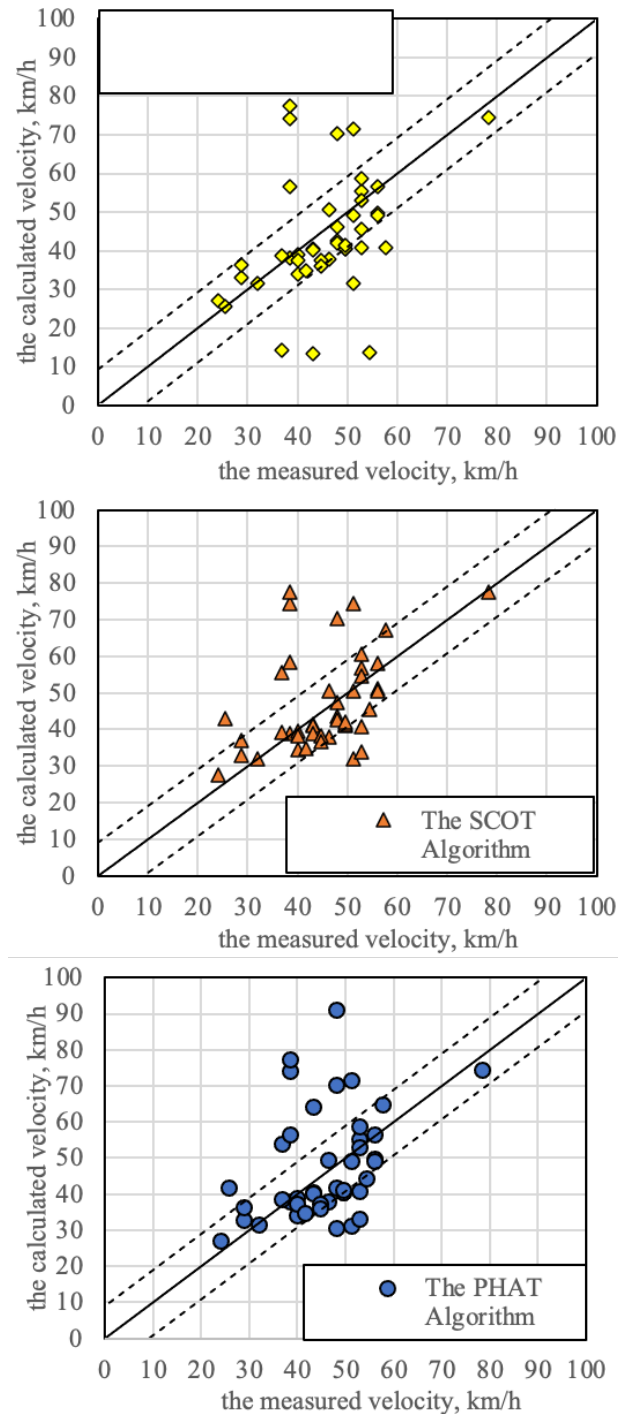
Figure 17. Comparison between the measured and the calculated velocity

The SNR and RE values are calculated to evaluate the reliability of the three cross-correlation algorithms, as listed in Table 8. It was found that the PHAT and the SCOT are more stable than the NCC algorithm, given their relatively high SNR value. The high SNR values indicate that the correlated and the independent noises are removed by the SCOT and the PHAT, respectively. In other words, the collected vertical stress data include correlated and independent noises. The SNR value of the PHAT is much larger than that of the SCOT. It indicates that there are more independent noises in the field test.

Table 8. The comparison of the cross-correlation algorithm with the field data

Index	NCC Algorithm	SCOT Algorithm	PHAT Algorithm
SNR	66.75±46.01	72.04±25.65	127.89±41.12
RE	0.29±0.33	0.22±0.24	0.25±0.25

Furthermore, the SCOT algorithm, compared with the PHAT algorithm, has better accuracy due to its low RE values. This indicates that the main parts of noises are correlated noise that could come from the test procedure (like the vibration of wheel loads, temperature change, etc.). This variation can be related to the variation of the vehicle speeds in the testing section and the measurement error of speed radar. Above all, the cross-correlation method can be used to estimate vehicle speed with reasonable stability and accuracy. The SCOT algorithm is recommended to analyze the test data.

CHAPTER 6

Modulus Estimation

The ANN model with a feed-forward structure was developed in Python 3.7. The inputs are amplitudes of the collected signals from the SmartRock including triaxial stress and Euler angle, loading frequency, and pavement temperatures. In the field, the collected data show non-stationary signals, hence they were analyzed by the empirical mode decomposition (EMD) method to remove the trend line and low-frequency noises (van Jaarsveldt et al., 2021). The output is the in-situ dynamic modulus under vehicular loading. The TanSig function compared with the sigmoid and ReLu function was chosen as the activation function. Hyperparameters of the ANN model were selected by the 5-fold cross-validation method. Consequently, a four-layer ANN model with fully connected nodes of different layers was developed. The lab data were used to select the model hyperparameters by the 5-fold cross-validation method. The laboratory data were randomly shuffled and divided into five groups. When a group was treated as a test set, other groups were used to train the model. The MRE was calculated for each test group. After 5 iterations the MRE for each group can be calculated. Table 5 shows the results of 5-fold cross-validation for the ANN model with different hyperparameters. For example, "8-4-1" means that the ANN model consists of three layers, including an 8-channel input layer, a 4-neuron hidden layer, and a 1-channel output layer. From Table 9 the ANN model has the lowest average MRE with the "8-6-4-1" structure, which is used to predict the in-situ dynamic modulus.

Table 9. Results of 5-fold cross-validation (MRE %)

No.	Hyperparameters	Testing Group 1	Testing Group 2	Testing Group 3	Testing Group 4	Testing Group 5	Average
1	8-4-1	39.41	126.58	8.79	12.52	29.16	44.26
2	8-5-1	17.47	280.02	36.93	11.27	28.69	74.88
3	8-4-2-1	45.94	42.3	9.3	24.65	30.43	30.52
4	8-6-4-1	38.00	17.01	3.46	28.82	28.42	23.14
5	8-6-6-1	285.37	11.00	17.60	23.30	26.86	72.83
6	8-6-4-2-1	36.81	100.38	9.34	44.35	30.21	44.12

This study only used the field data from the first two months for model development and calibration, to be compared with the laboratory dynamic modulus test results. During this period, the asphalt mixture is treated as new material and the in-situ modulus deterioration can be ignored given the short period and limited vehicular loading.

The training and testing datasets were built by different combinations of the lab and field data to evaluate the ANN model (Table 10). The first combination was applied to evaluate whether the ANN can predict the dynamic modulus with the collected data by SmartRock during laboratory testing. Combination 2, 3,

and 5 were used to evaluate the prediction for the in-situ dynamic modulus. Combination 5 was used to test the prediction of the dynamic modulus deterioration. The mean relative error (MRE) was calculated to evaluate the accuracy of prediction.

$$MRE = \frac{1}{n} \sum_{i=1}^{n} \frac{|Y_i - X_i|}{X_i} \times 100\% \tag{16}$$

Where: X_i and Y_i are the ith measured and predicted value. The n is the number of predicted values. The larger MRE indicates lower accuracy.

Table 10. The training and testing datasets

Combination	Training Dataset	Testing Dataset
1	Lab data	Lab data
2	Lab data and project A field data (first two weeks)	Project A field data (first and second month)
3	Lab data and project B field data (first two weeks)	Project B field data (first and second month)
4	Lab data and 80% field data (Project A and B)	MMLS3 deterioration data
5	Lab data and 80% field data (Project A and B)	MMLS3 data

PREDICTING DYNAMIC MODULUS WITH LAB DATA

The ANN model was trained by 80% of the laboratory data and tested by the remaining 20% of the laboratory data. Figure 18 shows the prediction results of the 20% testing data as compared to the measured results. The measured dynamic modulus is for the plant-mixed laboratory-compacted specimens. The predicted dynamic modulus are the ANN model predictions with the data collected by SmartRocks during dynamic modulus testing. The result (Figure 18) shows a prediction accuracy of MRE=24.8%, which indicates that the ANN model can reasonably predict the dynamic modulus using the SmartRock collected data.
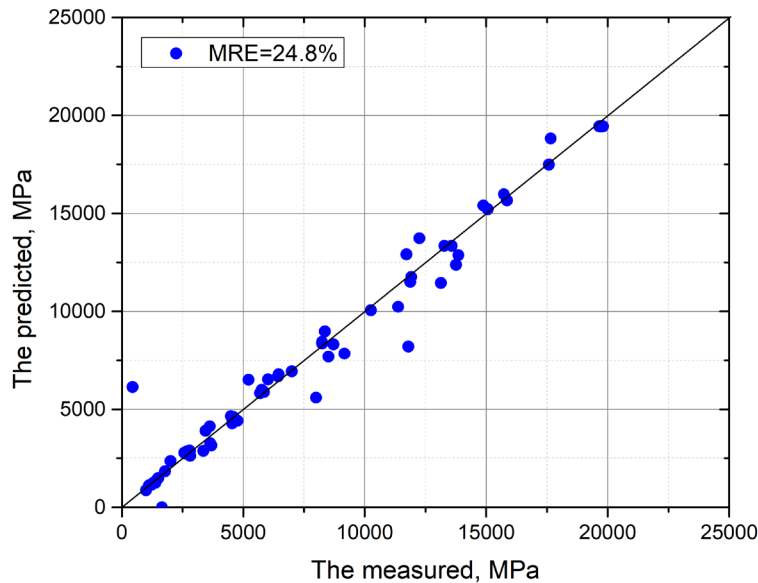
**Figure 18.** Model trained by lab data to predict lab data

PREDICTING IN-SITU DYNAMIC MODULUS IN PROJECT A

For project A, the training dataset consists of the field data collected during the first two weeks and the lab data. The field data collected during the first month and the second month were used to test the model. The accuracy of prediction is acceptable with 5.00% and 23.26% MRE, as shown in Figure 19(a) and 19(b), respectively.

The predicted dynamic modulus can be used to develop the master curve for pavement analysis. The recorded temperatures were used to obtain the shift factors to calculate the reduced frequencies, using 22 °C as the reference temperature. This reference temperature was selected for all master curves in this project to be consistent with the MMLS3 testing temperature. The parameters of the master curve (sigmoid model) can be regressed with the predicted modulus and reduced frequency, so that the modulus properties of the in-situ pavement at any temperature and frequency conditions can be obtained, which can be integrated into pavement analysis programs for maintenance decision making. The developed master curve for specific service period is shown in Figure 20. It is seen that due to limited range of frequency and temperature from the vehicular loading, the developed master curves only cover a narrow frequency band. In addition, the regression can be significantly influenced by the imprecision points that are located out of the MRE=30% outline. When the imprecision points are excluded from the regression, the regressed master curves are close to the measured master curve. It is clear that considering the high variation of the field data and conditions, the developed model is reasonable to predict the in-situ dynamic modulus with the SmartRock.
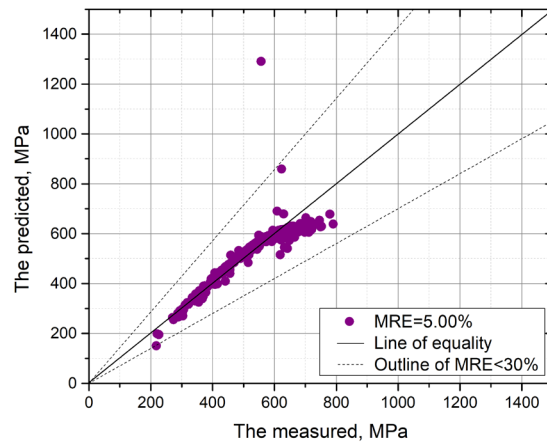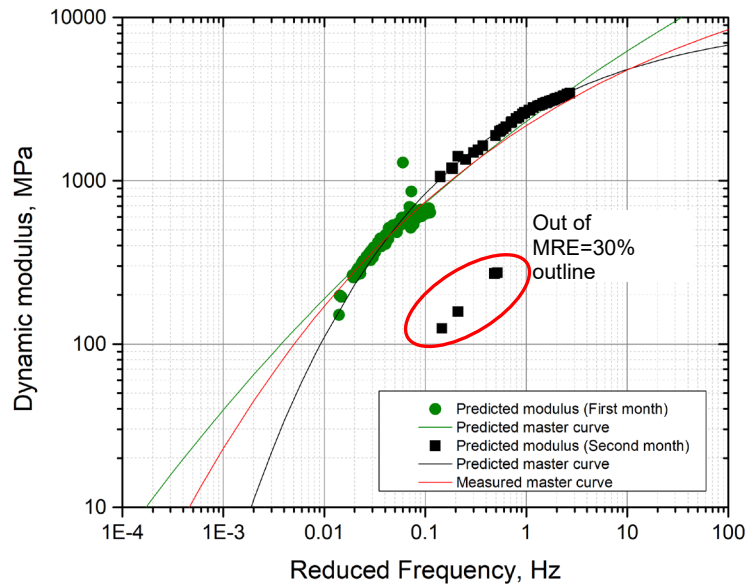
(a)
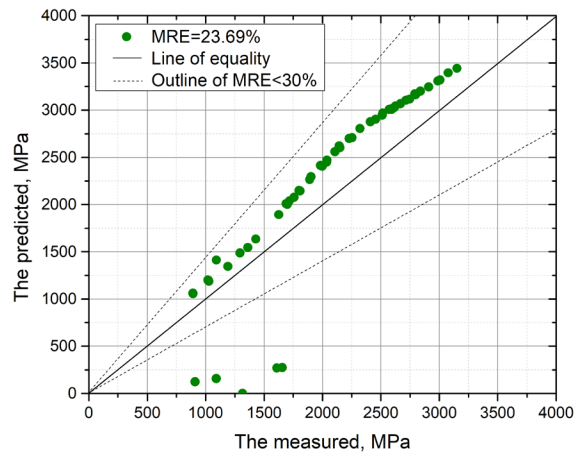
(b)

Figure 19. Prediction of the in-situ dynamic modulus in project A:
(a) at the first month, (b) at the second month

Figure 20. The regressed master curve of the in-situ dynamic modulus

PREDICTING IN-SITU DYNAMIC MODULUS IN PROJECT B

For project B, the field data collected during the first two weeks and the lab data were used to train the model. The field data collected during the first month and the second month were used to test the model. The accuracy of prediction is lower than that of project A but is still acceptable, with 14.17% and 27.72% MRE, as shown in Fig 21(a), 21(b).

The regressed master curves of the predicted dynamic modulus are shown in Figure 22. The master curve regressed by the first month data present a different trend with the measured master curve, because the prediction is in narrow frequency range. So, the wide frequency range of the collected data is required to obtain the master curve of the dynamic modulus. It also suggests that more field data with wider frequency and temperature ranges are needed in order to increase the accuracy and the robustness of the ANN model.

(a)

(b)

Figure 21. Prediction of the in-situ dynamic modulus in project 4:
(a) at the first month, (b) at the second month
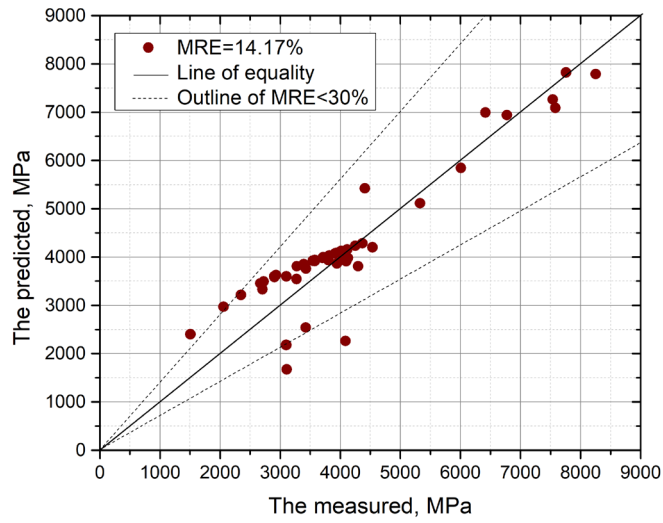
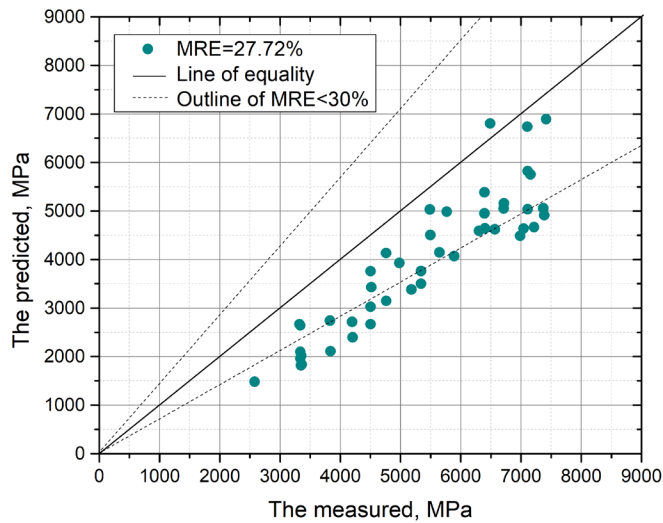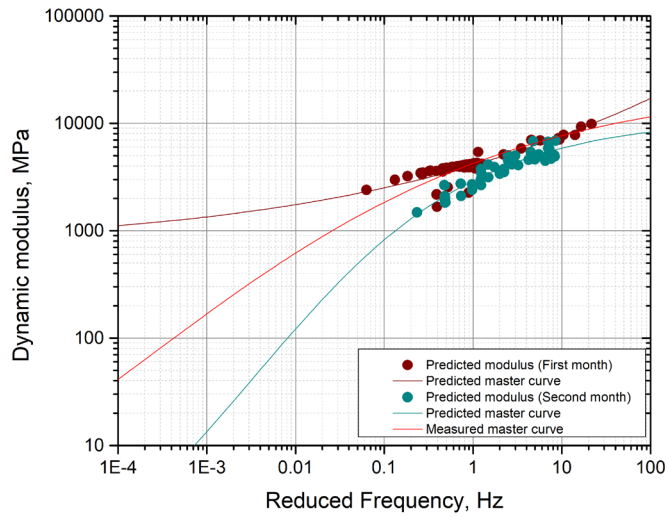**Figure 22.** The regressed master curve of the in-situ dynamic modulus

PREDICTING DYNAMIC MODULUS WITH MMLS3 DATA

This model was also applied to predict the dynamic modulus with the MMLS3 data. MMLS3 test is an accelerated simulation test that provides a condition of loading, boundary, and environment closer to the field condition as compared with the lab test. Therefore, 80% field data combined with all lab data were randomly chosen to train the model, and MMLS3 data were used solely to test the model. The dynamic moduli of asphalt mixture were predicted as shown in Figure 23. The measured values are the laboratory dynamic modulus of the plant-mixed laboratory-compacted specimens. The predicted values are the ANN model predictions with the field data collected by SmartRocks. The results show that the predictive model can reasonably predict the in-situ dynamic modulus with 13.47% MRE.
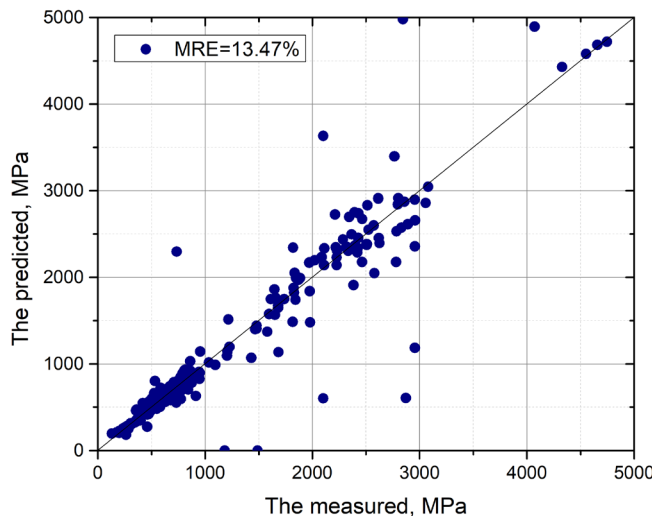
Figure 23. Prediction of the dynamic modulus for specimens under MMLS3 loading

PREDICTING DYNAMIC MODULUS DETERIORATION IN MMLS3 TEST

The MMLS3 data collected over time were used to test the predictive model and predict the dynamic modulus of the specimens in different deterioration conditions. Figure 24 shows the regressed master curves of the predicted dynamic modulus at different loading stages. As seen, these master curves are relatively close to each other, indicating the modulus properties didn't change significantly during the entire test.

The non-destructive test, UPV, was used in this study to verify the modulus change trend during the MMLS3 test. Figure 25 presents the change of dynamic modulus with the increase of loading passes, as a result of the UPV test at 22 ℃ temperature. The UPV test was performed at a high frequency (65,000 Hz), resulting in much higher dynamic moduli than those of laboratory tests. As shown in Figure 25, the UPV dynamic modulus shows an increasing trend with the number of loading passes, suggesting that the asphalt mixture is under secondary compaction. The specimens had no visual distress after a total of 71,716 load passes and only very minimal surface rut is seen, as shown in Figure 26. The measured moduli from the UPV tests are summarized in Table 11 at specific loading pass conditions. Also indicated in Table 11 are the predicted dynamic moduli values using the master curves obtained from the predictive models. As shown, in most cases the predicted dynamic modulus is higher than the UPV modulus. But both methods suggest that the modulus change trend over the 71,716 passes of loading is small and the material has very minimal damage. Figure 27 provides a visual presentation of the predicted master curves and the corresponding UPV modulus at specific loading passes.
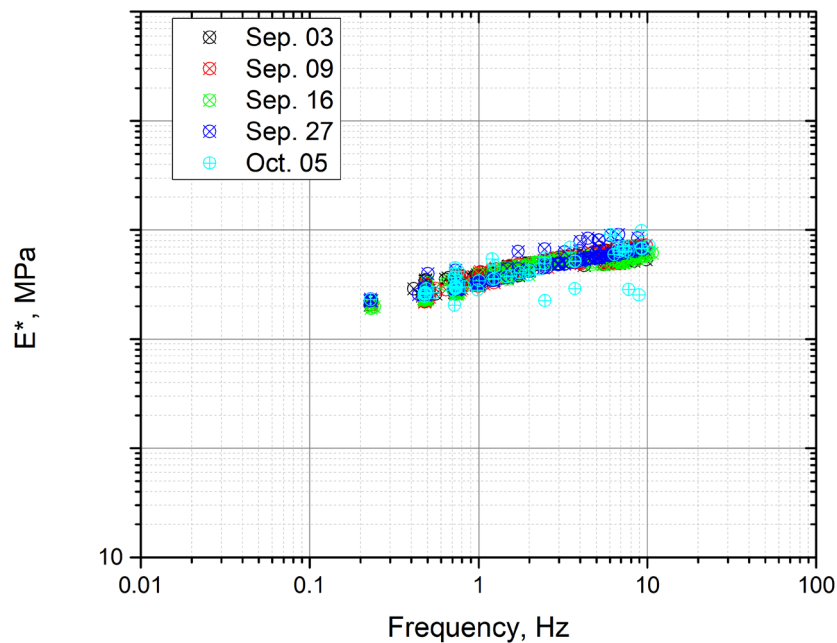
Figure 24. The regressed master curves of the dynamic modulus in MMLS3
(at 22 °C)
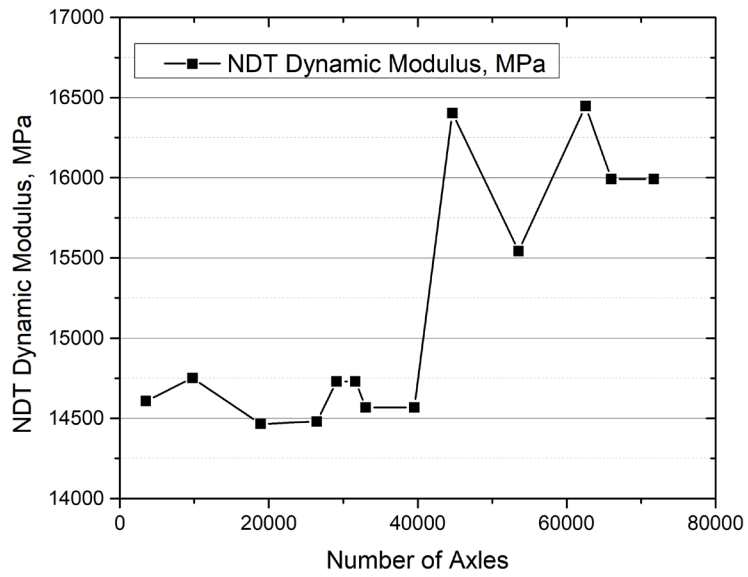
Figure 25. The change of the dynamic modulus in MMLS3 test
(65 000 Hz, 22 °C, from UPV test)

Figure 26. The specimens after the MMLS3 test

Table 11. Dynamic modulus in the MMLS3 from both NDT test and prediction

Date	Cumulative Axle Count	NDT Dynamic Modulus, MPa	Predicted Dynamic Modulus, MPa
3-Sep-21	3,518	14,607	21,677
7-Sep-21	9,771	14,751	26,112
9-Sep-21	18,883	14,465	24,988
10-Sep-21	26,464	14,479	7,913
14-Sep-21	29,121	14,731	15,409
16-Sep-21	31,631	14,731	8,650
22-Sep-21	33,035	14,568	26,998
27-Sep-21	39,527	14,568	25,678
30-Sep-21	53,553	15,543	26,888
5-Oct-21	62,534	16,446	23,286
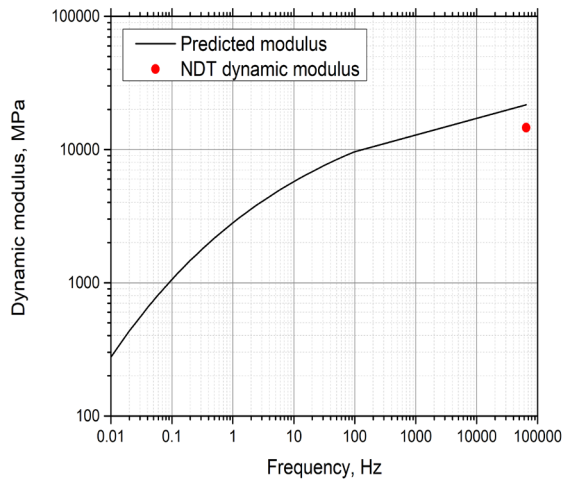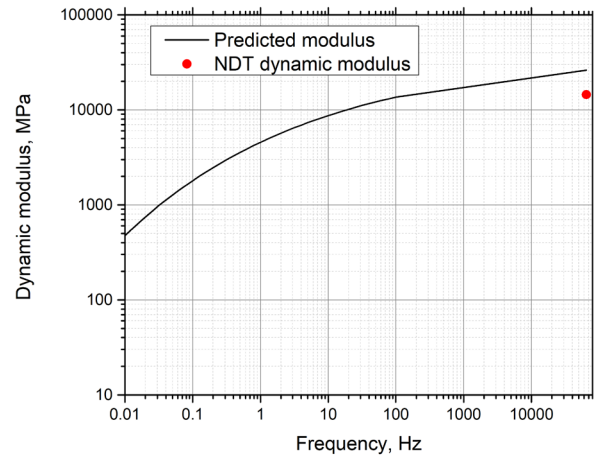
(a)   (b)

Figure 27. Projected master curves and the corresponding UPV modulus at (a) 3518 passes; (b) 18,883 passes

CHAPTER 7

Conclusions and Future Work

This project developed an in-situ dynamic modulus predictive model based on the ANN model using real-time sensing data. With the aid of embedded wireless sensors, an in-situ dynamic modulus test was proposed for field pavements based on real traffic and environmental conditions. Data collection and analysis strategies for particle size wireless sensors were introduced for roadway applications. Using the particle size wireless sensors, the mechanical responses of the pavement under vehicle loadings were successfully applied to estimate the traffic speed and the in-situ dynamic modulus of the asphalt pavement.

The in-situ modulus predictive model, when carefully trained by laboratory dynamic modulus and early-stage field data, can be used to predict the modulus trend (deterioration) over time based on the mechanistic responses of the in-situ pavement. Such information can thus be integrated into the pavement maintenance program for the assessment of pavement conditions and making cost-effective decisions for pavement maintenance or rehabilitation.

The loading speed is correlated to the duration of impulse and the dominant frequency, both of which have a crucial impact on the dynamic modulus. In this project, the vehicle speeds were estimated with the cross-correlation methods based on embedded SmartRock sensors. Three cross-correlation algorithms, the NCC algorithm, the SCOT algorithm, and the PHAT algorithm, were introduced.

The following conclusions were obtained based on this project, and some recommendations for future work are also summarized.

- The SmartRock sensor, a type of MEMS wireless sensor, can be used to collect the mechanical responses in the laboratory testing and in the field environment. Triaxial stress, triaxial Euler angle, loading frequency, and pavement temperature were found to be critical inputs for the predictive model.

- In the laboratory dynamic modulus test and the MMLS3 test, frequencies of the collected data can be obtained by the Fourier transform method. For the field data, the EMD method is needed to decompose the signals to obtain different intrinsic modes at characteristic frequencies.

- The ANN model is reasonable and reliable to estimate the in-situ dynamic modulus based on the data collected by SmartRock sensors. The MRE of the prediction is 13.47% for the test dataset, reasonably low for field conditions.

- The master curve of the in-situ dynamic modulus can be obtained by the predictions for pavement analysis. The quality of the field data and the range of the data (i.e., the temperature and frequency range) can significantly affect the master curve regression. Further studies are needed to improve the prediction accuracy.

- The material deterioration is a crucial factor for pavement condition assessment. Further research is needed to quantify the relationship between modulus deterioration and pavement condition. The effect of many other factors such as aging should also be considered in future studies.

- SmartRock sensors, when placed in series in the pavement, can be used to estimate the speed of the loading vehicles based on measured stress signals. In this study, the distance between two SmartRocks was 5.5 m in the field test. This distance is acceptable for the 20 km/h to 50 km/h speed range. Future studies are recommended to identify a suitable sensor distance for higher-speed traffic. The influences of distance, traffic wandering, and other factors on the speed estimation accuracy should also be evaluated in the future.

- The cross-correlation method can be used to estimate vehicle speed. The SCOT algorithm is recommended to estimate vehicle speed due to its relatively high SNR values and low RE values. The high SNR value indicates that the SCOT algorithm has better stability and is hardly influenced by abnormal values. The low RE value indicates that it has better accuracy for speed estimation.

- Based on the configuration of the field sensors, the number of cases in which the captured signals can be matched is 84.7% of the total number of cases. On the other hand, 15.3% of the results contained theoretical errors that contributed to RE values. Missing axle loads were found to be the source of the theoretical error. Therefore, increasing the ability to capture axle loads will improve the estimation accuracy. A strategy needs to be further researched to improve such data capturing capability and reliability of the sensor.

- The cross-correlation algorithms along with the embedded SmartRock wireless sensors were found to be a promising method for estimating the vehicles' speed in the field.

References

AASHTO T342 (2011). Standard method of test for determining dynamic modulus of hot mix asphalt (HMA).

Al-Qadi, I. L., Xie, W., & Elseifi, M. A. (2008). Frequency determination from vehicular loading time pulse to predict appropriate complex modulus in MEPDG. In *Asphalt Paving Technology-Proceedings*, *77*, 739.

American Association of State Highway and Transportation Officials. (2020). *Mechanistic-empirical pavement design guide: A manual of practice*. AASHTO.

Boyapati, B., & Kumar, R. P. (2015). Prioritisation of pavement maintenance based on pavement condition index. *Indian Journal of Science and Technology*, *8*(14), 1-5.

Burmister, D. M. (1945). The general theory of stresses and displacements in layered soil systems. III. *Journal of Applied Physics*, *16*(5), 296-302.

Dao, D. V., Nguyen, N. L., Ly, H. B., Pham, B. T., & Le, T. T. (2020). Cost-effective approaches based on machine learning to predict dynamic modulus of warm mix asphalt with high reclaimed asphalt pavement. *Materials*, *13*(15), 3272.

Darabi, M. K., Al-Rub, R. K. A., Masad, E. A., & Little, D. N. (2012). Thermodynamic-based model for coupling temperature-dependent viscoelastic, viscoplastic, and viscodamage constitutive behavior of asphalt mixtures. *International Journal for Numerical and Analytical Methods in Geomechanics*, *36*(7), 817-854.

Damirchilo, F., Hosseini, A., Mellat Parast, M., & Fini, E. H. (2021). Machine Learning Approach to Predict International Roughness Index Using Long-Term Pavement Performance Data. *Journal of Transportation Engineering, Part B: Pavements*, *147*(4), 04021058.

Carter, G. C., Nuttall, A. H., & Cable, P. G. (1973). The smoothed coherence transform. In *Proceedings of the IEEE*, *61*(10), 1497-1498.

Ceylan, H., Gopalakrishnan, K., Kim, S., Taylor, P. C., Prokudin, M., & Buss, A. F. (2013). Highway infrastructure health monitoring using micro-electromechanical sensors and systems (MEMS). *Journal of Civil Engineering and Management*, *19*(sup1), S188-S201.

Cheng, H., Wang, Y., Liu, L., & Sun, L. (2021). Relationships between asphalt-layer moduli under vehicular loading and FWD loading. *Journal of Materials in Civil Engineering*, *33*(1), 04020437.

Dimter, S., Rukavina, T., & Minažek, K. (2016). Estimation of elastic properties of fly ash-stabilized mixes using nondestructive evaluation methods. *Construction and Building Materials*, *102*, 505-514.

Hamim, A., Yusoff, N. I. M., Omar, H. A., Jamaludin, N. A. A., Hassan, N. A., El-Shafie, A., & Ceylan, H. (2020). Integrated finite element and artificial neural network methods for constructing asphalt concrete dynamic modulus master curve using deflection time-history data. *Construction and Building Materials*, *257*, 119549.

Hoang, N. D., Nguyen, Q. L., & Tien Bui, D. (2018). Image processing-based classification of asphalt pavement cracks using support vector machine optimized by artificial bee colony. *Journal of Computing in Civil Engineering*, *32*(5), 04018037.

Huff, R., Berthelot, C., & Daku, B. (2005). Continuous primary dynamic pavement response system using piezoelectric axle sensors. *Canadian Journal of Civil Engineering*, *32*(1), 260-269.

Iaquinta, J., Merliot, E., Cottineau, L. M., & Desroche, J. P. (2004). Piezoelectric sensors for weigh-in-motion systems: An experimental insight into edge effects. *Journal of Testing and Evaluation*, *32*(6), 476-483.

Islam, M. R., Hossain, M. I., & Tarefder, R. A. (2014). Field validation of the arching phenomenon of earth pressure cell to measure vertical stress in flexible pavement. In *Advanced Characterization of Asphalt and Concrete Materials* (pp. 99-106).

Ismaili Alaoui, E. M., & Ibn-Elhaj, E. (2017). A comparative study of new HOS-based estimators for moving objects in noisy video sequence. *Signal, Image and Video Processing*, *11*(7), 1297-1304.

Karballaeezadeh, N., Mohammadzadeh, S. D., Moazemi, D., Band, S. S., Mosavi, A., & Reuter, U. (2020). Smart structural health monitoring of flexible pavements using machine learning methods. *Coatings*, *10*(11), 1100.

Knapp, C., & Carter, G. (1976). The generalized correlation method for estimation of time delay. *IEEE transactions on acoustics, speech, and signal processing*, *24*(4), 320-327.

Kutay, M. E., Chatti, K., & Lei, L. (2011). Backcalculation of dynamic modulus mastercurve from falling weight deflectometer surface deflections. *Transportation Research Record*, *2227*(1), 87-96.

Liu, S., Huang, H., & Qiu, T. (2015, March). Laboratory development and testing of "SMARTROCK" for railroad ballast using discrete element modeling. In *ASME/IEEE Joint Rail Conference* (Vol. 56451, p. V001T01A019), American Society of Mechanical Engineers.

Majidifard, H., Adu-Gyamfi, Y., & Buttlar, W. G. (2020). Deep machine learning approach to develop a new asphalt pavement condition index. *Construction and Building Materials*, *247*, 118513.

Mo, L., Li, C., Huang, H., & Dong, Y. (2018). A Study of Walking Speed Measurement for Elderly Health Assessment Using Ultrahigh-frequency Radio-frequency Identification Tags. *Sens. Mater.*, *30*, 1039-1051.

Papagiannakis, A. T., Phang, W. A., Woodrooffe, J. H. F., Bergan, A. T., & Haas, R. C. G. (1989). Accuracy of weigh-in-motion scales and piezoelectric cables. *Transp. Res. Record*, *1215*, 189-196.

Praticò, F. G., Fedele, R., Naumov, V., & Sauer, T. (2020). Detection and monitoring of bottom-up cracks in road pavement using a machine-learning approach. *Algorithms*, *13*(4), 81.

Rahman, M. M., & Tarefder, R. A. (2015). PCI and non-PCI-based pavement evaluation. *Journal of Airport Management*, *9*(2), 185-196.

Saafi, M., & Romine, P. (2005). Preliminary evaluation of MEMS devices for early age concrete property monitoring. *Cement and Concrete Research*, *35*(11), 2158-2164.

Sebaaly, P. E., Tabatabaee, N., & Kulakowski, B. (1995). Evaluation of the Hall Effect sensor for pavement instrumentation. *Journal of Testing and Evaluation*, *23*(3), 189-195.

Spagnolini, U. (2018). *Statistical Signal Processing in Engineering*. John Wiley & Sons.

Tabatabaee, N., & Sebaaly, P. (1990). State-of-the-art pavement instrumentation. *Transportation Research Record*, *1260*, 246-255.

Teral, S. (1992). Vehicle weighing in motion with fiber optic sensors. In *First European Conference on Smart Structures and Materials* (Vol. 1777, p. 17770S), International Society for Optics and Photonics.

Theroux, B., Labuz, J. F., & Dai, S. (2001). Field installation of an earth pressure cell. *Transportation Research Record*, *1772*(1), 12-19.

Tsai, D. M., & Lin, C. T. (2003). Fast normalized cross correlation for defect detection. *Pattern Recognition Letters*, *24*(15), 2625-2631.

Uzan, J. (1994). Dynamic linear back calculation of pavement material parameters. *Journal of Transportation Engineering*, *120*(1), 109-126.

van Jaarsveldt, C., Peters, G., Ames, M., & Chantler, M. J. (2021). Tutorial on Empirical Mode Decomposition: Basis Decomposition and Frequency Adaptive Graduation in Non-Stationary Time Series. *Available at SSRN 3913330*.

Wang, H., Liu, W., He, J., Xing, X., Cao, D., Gao, X., Hao, X., Cheng, H., & Zhou, Z. (2014). Functionality enhancement of industrialized optical fiber sensors and system developed for full-scale pavement monitoring. *Sensors*, *14*(5), 8829-8850.

Wang, H., Li, M., Szary, P., & Hu, X. (2019). Structural assessment of asphalt pavement condition using backcalculated modulus and field data. *Construction and Building Materials*, *211*, 943-951.

Wang, X., Shen, S., Huang, H., & Almeida, L. C. (2018). Characterization of particle movement in Superpave gyratory compactor at meso-scale using SmartRock sensors. *Construction and Building Materials*, *175*, 206-214.

Wang, X., Shen, S., Huang, H., & Zhang, Z. (2019). Towards smart compaction: Particle movement characteristics from laboratory to the field. *Construction and Building Materials*, *218*, 323-332.

Zhang, C., Shen, S., Huang, H., & Wang, L. (2021). Estimation of the vehicle speed using cross-correlation algorithms and MEMS wireless sensors. *Sensors*, *21*(5), 1721.

Zeiada, W., Dabous, S. A., Hamad, K., Al-Ruzouq, R., & Khalil, M. A. (2020). Machine learning for pavement performance modelling in warm climate regions. *Arabian Journal for Science and Engineering*, *45*(5), 4091-4109.

Zhou, S., Tang, B., & Chen, R. (2009). Comparison between non-stationary signals fast Fourier transform and wavelet analysis. In *2009 International Asia Symposium on Intelligent Interaction and Affective Computing* (pp. 128-129), IEEE.